

1 **Chemical composition, optical properties, and oxidative potential of water-**
2 **and methanol-soluble organic compounds emitted from the combustion of**
3 **biomass materials and coal**

4

5 Tao Cao^{1,3}, Meiju Li^{1,3}, Chunlin Zou^{1,3}, Xingjun Fan⁴, Jianzhong Song^{1,2,5,*}, Wanglu, Jia^{1,2},
6 Chiling Yu^{1,2}, Zhiqiang Yu^{1,2}, Ping'an Peng^{1,2,3,5}

7

8 ¹State Key Laboratory of Organic Geochemistry and Guangdong Provincial Key Laboratory
9 of Environmental Protection and Resources Utilization, Guangzhou Institute of Geochemistry,
10 Chinese Academy of Sciences, Guangzhou 510640, China

11 ²CAS Center for Excellence in Deep Earth Science, Guangzhou, 510640, China

12 ³University of Chinese Academy of Sciences, Beijing 100049, China

13 ⁴College of Resource and Environment, Anhui Science and Technology University, Anhui
14 233100, China

15 ⁵Guangdong-Hong Kong-Macao Joint Laboratory for Environmental Pollution and Control

16

17 **Correspondence to:* Jianzhong Song (songjzh@gig.ac.cn)

18

19 **Abstract**

20 Biomass burning (BB) and coal combustion (CC) are important sources of brown carbon
21 (BrC) in ambient aerosols. In this study, six biomass materials and five types of coal were
22 combusted to generate fine smoke particles. The BrC fractions, including water-soluble
23 organic carbon (WSOC), humic-like substance-carbon (HULIS-C), and methanol-soluble
24 organic carbon (MSOC), were subsequently fractionated, and their optical properties and
25 chemical structures were then comprehensively investigated using UV-visible spectroscopy,
26 proton nuclear magnetic resonance spectroscopy ($^1\text{H-NMR}$), and fluorescence
27 extraction-emission matrix spectroscopy (EEM) combined with parallel factor analysis
28 (PARAFAC). In addition, the oxidative potential (OP) of BB and CC BrC was measured with
29 the dithiothreitol (DTT) method. The results showed that WSOC, HULIS-C, and MSOC
30 accounted for 2.3%–22%, 0.5%–10%, and 6.4%–73% of the total mass of
31 combustion-derived smoke $\text{PM}_{2.5}$, respectively, with MSOC extracting the highest
32 concentrations of organic compounds. The MSOC fractions had the highest light absorption
33 capacity (mass absorption efficiency at 365 nm (MAE_{365}): 1.0–2.7 m^2/gC) for both BB and
34 CC smoke, indicating that MSOC contained more of the strong light-absorbing components.
35 Therefore, MSOC may represent the total BrC better than the water-soluble fractions. Some
36 significant differences were observed between the BrC fractions emitted from BB and CC
37 with more water-soluble BrC fractions with higher MAE_{365} and lower absorption Ångström
38 exponent values detected in smoke emitted from BB than from CC. EEM-PARAFAC
39 identified four fluorophores: two protein-like, one humic-like, and one polyphenol-like. The
40 protein-like substances were the dominant components of WSOC (47%–80%), HULIS-C

41 (44%–87%), and MSOC (42%–70%). The ¹H-NMR results suggested that BB BrC contained
42 more oxygenated aliphatic functional groups (H-C-O) whereas CC BrC contained more
43 unsaturated fractions (H-C-C = and Ar-H). The DTT assays indicated that BB BrC generally
44 had a stronger oxidative potential (DTT_m, 2.6–85 pmol/min/μg) than CC BrC (DTT_m, 0.4–11
45 pmol/min/μg), with MSOC having a stronger OP than WSOC and HULIS-C. In addition,
46 HULIS-C contributed more than half of the DTT activity of WSOC (63.1%±15.5%),
47 highlighted that HULIS was a major contributor of ROS production in WSOC. Furthermore,
48 the Principal component analysis and Pearson correlation coefficients indicated that highly
49 oxygenated humic-like fluorophore C4 may be the important DTT active substances in BrC.

50

51

52

53 **1. Introduction**

54 Brown carbon (BrC) is an organic compound with strong light absorption at ultraviolet
55 and short visible wavelengths and is abundant in ambient aerosols (Chen and Bond, 2010;
56 Laskin et al., 2015; Alexander et al., 2008), rain, clouds, and fog water (Santos et al., 2009;
57 Santos et al., 2012; Izhar et al., 2020). Due to its strong light absorption ability, BrC can
58 affect the radiative balance of aerosol and photochemical reactions in the atmospheric
59 environment (Andreae and Gelencser, 2006; Kumar et al., 2018a; Nozière et al., 2011).
60 Moreover, BrC has the ability to catalyze the generation of reactive oxygen species (ROS),
61 which potentially have an adverse impact on human health (Bates et al., 2019; Ma et al., 2018;
62 Fan et al., 2018; Chen et al., 2019).

63 Brown carbon originates from various sources, including primary emission sources, such
64 as biomass burning (BB), coal combustion (CC), and vehicular emissions (Fan et al., 2018; Li
65 et al., 2018; Chen et al., 2019; Sun et al., 2017); and secondary processes, such as reactions
66 between carbonyls and ammonia or amines and the photochemical transformation of volatile
67 organic compounds (Evangelidou et al., 2019; Lin et al., 2015). Among these sources, BB and
68 CC are considered to make significant contributions to atmospheric BrC materials as
69 indicated in both laboratory and field studies (Li et al., 2018; Park and Yu, 2016; van der Werf
70 et al., 2010; Yan et al., 2015). For example, BrC fractions, such as water-soluble organic
71 carbon (WSOC), humic-like substance-carbon (HULIS-C), and methanol-soluble organic
72 carbon (MSOC), have been found to be abundant in fresh emissions from the burning of crop
73 straw, wood branches, and coals (Park and Yu, 2016; Fan et al., 2018; Li et al., 2018; Huo et
74 al., 2018). These studies have also demonstrated that the chemical properties of primary BrC

75 are variable due to the inherent heterogeneity and complexity of fuel materials and
76 combustion conditions (Huo et al., 2018; Fan et al., 2018; Li et al., 2018; Atwi et al., 2021).
77 For example, the light absorption properties of primary HULIS-C produced by the
78 combustion of three types of crop straw under different moisture contents and stacking modes
79 are different. The absorption Ångström exponent (AAE) increased and the mass absorption
80 efficiency at 365 nm (MAE_{365}) decreased under high moisture or stacking conditions (Huo et
81 al., 2018). The water-soluble BrC emitted from low maturity CC generally had relatively low
82 MAE_{365} values (Li et al., 2018). However, most of these studies only focused on the relative
83 abundances, chemical composition, and optical properties of water-soluble BrC (e.g., HULIS)
84 emitted from the combustion of various fuels and different combustion conditions (e.g.,
85 smoldering and flaming) (Huo et al., 2018; Park et al., 2016; Fan et al., 2016). It is noted that
86 water-insoluble BrC even exhibits a higher light absorption than water-soluble BrC in
87 ambient aerosols (Chen et al., 2016, 2017; Bai et al., 2020; Huang et al., 2020; Li et al., 2019).
88 However, knowledge on the chemical and optical properties of water-insoluble BrC from
89 combustion sources is still lacking. Moreover, the association of chemical compositions
90 responsible for light absorption of BrC from combustion sources is still constrained.
91 Therefore, to gain more detailed information on BrC from combustion sources, a
92 comprehensive characterization, including the chemical and optical characteristics of the BrC
93 fractions (including both water-soluble and water-insoluble BrC) from the combustion of
94 biomass materials and coals, is required.

95 In addition, the oxidative potential (OP) of water-soluble organic fractions (WSOC and
96 HULIS) and the water-insoluble organic fraction in ambient aerosols have been investigated,

97 and all are known to be significant redox-active organic compounds associated with ROS
98 generation, which can adversely affect human health (Moufarrej et al., 2020; Bates et al.,
99 2019; Verma et al., 2012; Kramer et al., 2016; Wong et al., 2019). As important contributors
100 to ambient BrC, combustion-derived BrC is expected to have a strong ROS generation
101 capacity and be harmful to human health. For example, the oxidative potential of the
102 water-soluble fraction of atmospheric fine aerosols were analyzed and revealed that biomass
103 burning dominates the ROS-generation potential in winter, contributing more than 46% to
104 DTT activities in the southeastern United State (Verma et al., 2014) and 41% in Milan, Italy
105 (Hakimzadeh et al., 2020). In addition, study on the oxidative potential of water-soluble
106 HULIS in fine aerosols in Beijing also indicated that combustion sources contributed a high
107 proportion to the oxidative stress of water-soluble HULIS fractions (Ma et al., 2018).
108 However, these results were mainly obtained based on the source apportionment receptor
109 model (positive matrix factorization (PMF) and chemical mass balances (CMB)). Recently,
110 the water extracts and HULIS from biomass burning were directly investigated and presented
111 significant oxidative potential to generate ROS (e.g., 6.6-55 pmol/min/ μ g for WSOC and
112 HULIS extracted from biomass burning smokes) (Fan et al., 2018; Pietrogrande et al., 2021;
113 Seo et al., 2020). In addition, high oxidative potentials (2.04-15.5 pmol/min/ μ g) were also
114 observed for water extracts in soots generated from the combustion of fossil fuels (Li et al.,
115 2019; Zhu et al., 2019). However, this limited studies only focused on the water-soluble BrC
116 fraction from biomass burning; and knowledge on the oxidative potential of the
117 water-insoluble BB BrC and BrC fractions emitted from other combustion processes, such as
118 coal combustion, is still lacking. In addition, the DTT activities of BrC from different

119 combustion sources were generally different, but the key components or functional groups
120 that responsible for the ROS generation capacity of combustion-derived BrC are unclear.

121 Biomass fuels and coals are two traditional sources of energy in residential properties in
122 some developing countries, especially China and India (Sun et al., 2017; Huo et al., 2018;
123 Singh et al., 2021). Due to incomplete combustion and poor pollution control, BB and CC
124 release various pollutants, including particulate matter (PM), elemental carbon (EC), and BrC.
125 In this study, we investigated the optical properties, chemical composition, and oxidative
126 potential of BrC fractions in smokes emitted from BB and CC. Six biomass materials (three
127 types of crop straw and three types of wood branches) and five coals with different maturities
128 were combusted, and the resulting smoke particles were collected in a laboratory combustion
129 chamber. The water soluble (WSOC and HULIS-C) and methanol soluble (MSOC) fractions
130 in smoke were fractionated using pure water combined with solid-phase extraction (SPE) and
131 methanol extraction. Subsequently, their chemical and optical properties were measured using
132 a total organic carbon analyzer, UV-visible spectroscopy, fluorescence extraction-emission
133 matrix spectroscopy (EEM) combined with parallel factor analysis (PARAFAC), and proton
134 nuclear magnetic resonance spectroscopy ($^1\text{H-NMR}$). Moreover, the oxidative potential of the
135 BrC fractions was determined by a dithiothreitol (DTT) assay. This is a comprehensive study
136 of the chemical and optical properties of BrC fractions, including both water-soluble and
137 water-insoluble fractions from BB and CC. The OP of different BrC fractions from BB and
138 CC were directly determined, and the key components or properties associated with the OP of
139 BrC were further discussed. The information obtained will enhance our understanding of the
140 chemical composition, light absorption, fluorophores, and DTT activity of the primary BrC

141 from BB and CC and could be used to estimate the environmental and climate impacts of
142 different types of combustion-derived BrC.

143

144 **2. Materials and methods**

145 **2.1. The BB and CC smoke samples**

146 In this study, six biomass materials and five types of coal were collected and used to
147 generate smoke samples. The biomass materials consisted of three types of crop straw (wheat
148 straw (WS), rice straw (RS), and corn straw (CS)) and three types of wood branches (pine
149 wood (PW), Chinese fir (CF), and white poplar (WP)). These materials are usually used as
150 fuels for heating and cooking in rural areas and are also occasionally burned in the field (Fan
151 et al., 2018; Kumar et al., 2018b). The combustion of these crop straws and woody fuels is
152 reported to make a significant contribution to atmospheric aerosols in China (Shen et al.,
153 2013). Five types of coal were used for the collection of CC smoke samples. They consisted
154 of four types of bituminous coal (B-1, B-2, B-3, and B-4) and one anthracite coal (AN),
155 representing the major types of coal used for residential CC in China. The details of these
156 samples are provided in the supporting information (SI).

157 Samples of the smoke emitted from BB and CC were collected in a combustion and
158 sampling system. The system consisted of a combustion hood, clean background air dilution
159 and injection ports, smoke pipe, mixing fan, mixing chamber, PM_{2.5} sampler (JCH-120F,
160 Juchuang Environmental Protection Group Co., Ltd., Shandong, China), and an exhaust port.
161 The details of the sampling procedure are described in our previous study (Fan et al., 2018; Li
162 et al., 2018) and the SI file.

163 Blank quartz filters were collected before each group of combustion experiments prior to
164 the fuels being ignited. Blank filters were used to correct the mass of smoke, the optical
165 signals and DTT consumption by BrC. To prevent contamination of the following sample, the
166 collection system was cleaned before each new combustion experiment.

167

168 **2.2. Extraction and isolation of BrC fractions**

169 In this study, the WSOC, HULIS-C, and MSOC fractions were obtained using the
170 solvent extraction method, as described in our previous studies (Fan et al., 2016; Li et al.,
171 2018). Initially, the filter samples were cut into small pieces and ultrasonically extracted three
172 times with 20 mL ultrapure water for 30 min. The extract was filtered through a 0.22 μm
173 polytetrafluoroethylene (PTFE) syringe filter (Jinteng, Tianjin, China), which collected the
174 WSOC fraction. The HULIS-C fraction in WSOC was further isolated using the SPE (Oasis
175 HLB, 200 mg, Waters, Milford, MA, USA) method. The detailed procedure is provided in S3
176 of SI file.

177 The MSOC fraction was obtained using a method developed by Cheng et al. (2016).
178 Briefly, a portion of the filter was immersed in methanol (Macklin, >99.9%, Shanghai, China)
179 for 2 h and then filtered through a 0.22 μm PTFE syringe filter. Static digestion without
180 ultrasonic treatment can avoid the loss of PM and facilitate the determination of the dissolved
181 organic matter (DOM) content. Finally, the residual filters were dried in a vacuum dryer. The
182 OC content of MSOC was obtained by subtracting the OC concentration of the extracted
183 filters from untreated filters.

184

185 **2.3. UV-visible spectroscopy**

186 The UV-visible absorption spectra of the BrC solutions were analyzed using a UV-vis
187 spectrophotometer (UV-2600, Shimadzu, Kyoto, Japan). The BrC solution was placed in a
188 0.01 m quartz cuvette, and the UV-vis spectra were recorded from 200 to 700 nm at 1 nm
189 intervals. Milli-Q water was used as a blank reference for the WSOC and HULIS-C solutions
190 while pure methanol was used as the blank for the MSOC fraction. The corresponding
191 background was used to determine the interference from the instrument and operational blank
192 sample.

193 To describe the optical properties of BrC fractions, the AAE and MAE₃₆₅ were calculated
194 in this study. The AAE is a measure of the spectral dependence of chromophores in BrC while
195 the MAE₃₆₅ can indicate the light absorbing capacity of BrC (Fan et al., 2016; Cheng et al.,
196 2016). The detailed calculations are described in the SI file.

197

198 **2.4. Fluorescence EEM spectroscopy and the PARAFAC model**

199 The EEM fluorescence spectra of BrC fractions were recorded by an F-4600
200 fluorescence spectrometer (Hitachi, Tokyo, Japan) using a 0.01 m width quartz cuvette with a
201 400 V xenon lamp at room temperature and a 2400 nm/min scanning speed. The scanning
202 ranges for excitation (E_X) and emission (E_M) were 200–400 nm and 290–520 nm, respectively.
203 The slit width and intervals for E_X and E_M were both set to 5 nm. According to the different
204 solvents used for sample extraction (water and methanol), all EEM spectra were divided into
205 two groups for analysis (66 samples for water-soluble WSOC and HULIS-C and 33 samples
206 for MSOC). The PARAFAC modeling procedure was conducted in EFC v1.2, which is an

207 application software based on MATLAB that has the functions of conversion, correction,
208 cognition, comparison, and calculation for processing the fluorescence spectra (He and Hur,
209 2015; Murphy et al., 2011; Murphy et al., 2013). The PARAFAC analysis method that was
210 included in the software was consistent with the calculation made by the drEEM toolkit when
211 using MATLAB (Murphy et al., 2010; Murphy et al., 2013). The PARAFAC was computed
212 using two to seven component models, with nonnegativity constraints and a residual analysis;
213 and split half analysis was used to validate the number of fluorescence components.
214 According to the results of the split-half and core consistency analysis, four component
215 models were chosen for both the WSOC and HULIS-C fractions and the MSOC. The EEM
216 was normalized to the area under the ultrapure water Raman peak ($E_X = 350$ nm, $E_M = 365$ –
217 430 nm) collected before the measurement of samples to produce corrected fluorescence
218 intensities in Raman units (Lawaetz and Stedmon, 2009). The relative contribution of
219 individual chromophores was estimated by calculating the maximum fluorescence intensities
220 (F_{\max} : maximum fluorescence intensity of identified fluorescence components, relative
221 content % = $F_{\max}/\Sigma F_{\max}$) (Matos et al., 2015; Chen et al., 2016).

222

223 **2.5. Proton-NMR spectroscopy**

224 Approximately 5 mg of the BrC fractions (i.e., HULIS-C, WSOC, and MSOC) derived
225 from BB and CC were used for ^1H NMR measurements. The water-soluble BrC fractions
226 (WSOC and HULIS-C) were redissolved in 500 μL deuterium oxide, and MSOC was
227 redissolved in 500 μL deuterated methanol and then transferred to a 5 mm NMR tube.
228 ^1H -NMR spectra were obtained at a frequency of 400 MHz using a spectrometer (Avance III

229 400, Bruker Daltonik GmbH, Bremen, Germany). Data were acquired from 100 scans, with a
230 recycling time of 2 s for a condensed water sample. The length of the proton 90° pulse was
231 8.87 μ s. A 1.0 Hz line-broadening weighting function and baseline correction were applied.
232 The identification of the functional groups in the NMR spectra was based on their chemical
233 shift (δ H) relative to that of tetramethylsilane (0 ppm), which was applied as an internal
234 standard (Zou et al., 2020).

235

236 **2.6. Oxidative potential**

237 The oxidative potential of BrC emitted from the BB and CC processes (i.e., WSOC,
238 HULIS-C, and MSOC) was measured by a DTT assay. This protocol was mainly followed the
239 methods introduced by Fan et al (2018) and Gao et al (2020), and also with some minor
240 modifications. Briefly, 3 mL of extracted sample solution (MSOC was a mixture of 100 μ L
241 sample and 2.9 mL of 18.2 M Ω Milli-Q water, and the corresponding blank was the same
242 solution as that of the water blank) and 3 mL of 1 mM DTT were mixed in a 20 mL brown
243 vial and then placed in a 37 °C water bath to maintain the samples at a constant temperature.
244 At specific time intervals (0, 5, 10, 15, and 20 min), 1 mL of the well-mixed sample was
245 transferred to another 4 mL brown vial, and 1 ml trichloroacetic acid (TCA 1% w/v) was
246 added to stop the reaction. Then, 0.5 mL 5,5'-dithiobis-(2-nitrobenzoic acid) (DTNB, 1 mM)
247 was added to react with the remaining DTT to produce 2-nitro-5-thiobenzoic acid (TNB).
248 After 5 min, 1 mL of tris(hydroxymethyl)methyl aminomethane buffer (0.4 mM Tris buffer,
249 pH 8.9 in 4 mM) containing diethylene triamine pentaacetic acid (DTPA) was added, and the
250 yellow color of TNB was visible in the mixed samples. The absorbance was measured at 412

251 nm with a UV-vis spectrometer (UV2600, Shimadzu). The DTT, TCA, and DTNB were all
252 dissolved in 0.1 M phosphate buffer (pH 7.4) containing 1 mM DTPA. and the corresponding
253 filter blank was analyzed to correct the DTT activity of the sample fractions. The DTT
254 consumption rate after subtracting the field blank was determined using the absorbance and
255 normalized by the particulate mass (DTT_m , pmol/min/ μ g) (Verma et al., 2012; Fan et al.,
256 2018). In this study, 1,4-phenanthraquinone was used to conduct a positive control, of which
257 the DTT consumption rate was $0.46 \pm 0.03 \mu\text{M DTT}/\text{min}$ (n=10). The rate was similar to
258 those reported in the previous studies (Fan et al., 2018; Lin and Yu, 2019).

259

260 **3. Results and discussion**

261 **3.1. Abundance of WSOC, HULIS-C, and MSOC in BB and CC smoke samples**

262 Table 1 summarizes the abundance of BrC fractions, including WSOC, HULIS-C, and
263 MSOC, in BB and CC smoke $PM_{2.5}$ samples. As shown in Table 1, the average contribution
264 of WSOC to smoke $PM_{2.5}$ was 2.9%–12% and 2.3%–22% for BB and CC, respectively. These
265 results were comparable to the results obtained for smoke samples from the combustion of
266 cherry leaves (16%), ginkgo tree leaves (6.0%) (Park et al., 2013), corn straw (5.9%), pine
267 branches (6.4%) (Fan et al., 2016), and residential coals (4%–11%) (Li et al., 2018) and in the
268 ambient $PM_{2.5}$ from rural and urban sites (4–13%) (Matos et al., 2015; Qin et al., 2018; Wu et
269 al., 2020). This suggests that both BB and CC can release substantial amounts of
270 water-soluble BrC into atmospheric aerosols. As the hydrophobic fraction of WSOC, the
271 carbon content of HULIS (HULIS-C) accounted for 1.0%–7.8% and 0.5%–10% of BB and
272 CC smoke $PM_{2.5}$, respectively. These values are comparable to the results obtained for BB

273 smoke (5.9%–15.2%) (Fan et al., 2018; Huo et al., 2018), CC smoke (1.9%–4.8%) (Li et al.,
274 2018), and atmospheric aerosols in Beijing (4.8%–9.4%) (Li et al., 2019), with an average
275 value of $7.2\% \pm 3.3\%$, therefore confirming the important contributions made by BB and CC
276 to atmospheric HULIS. As a comparison, the contribution of MSOC to smoke $PM_{2.5}$ was
277 6.4%–47% and 9.4%–73% for BB and CC, respectively, with both values being much higher
278 than the contributions of the water-soluble fractions (WSOC and HULIS-C) in the same
279 smoke samples. Similar results have been reported in previous studies (Li et al., 2018; Cheng
280 et al., 2016), which suggest that there are more organic compounds that could be extracted by
281 methanol than by water, and it could therefore be a better indicator of total BrC. This result
282 also indicated that BB and CC both released large amounts of water-insoluble BrC
283 compounds, including hydrophobic polycyclic aromatic hydrocarbons (PAHs) and
284 nitrogen/sulfur-containing heteroatomic PAHs (Geng et al., 2014; Dong et al., 2021; Huang et
285 al., 2020).

286 Some differences were observed among the different types of smoke samples. As shown
287 in Figure 1, the average contributions of the WSOC and HULIS-C fractions to the total
288 carbon (TC) were $22\% \pm 7.3\%$ and $11\% \pm 3.8\%$, respectively, for BB smoke, which were
289 higher than the corresponding values of $19\% \pm 9.4\%$ and $8.2\% \pm 4.0\%$ for CC smoke. The
290 contribution of MSOC to OC was $69\% \pm 19\%$ for BB, which was significantly lower than the
291 value of $97\% \pm 1.8\%$ for CC. These results suggested that BB generally released the more
292 water-soluble OC fraction whereas more water-insoluble OC fraction was contained in the
293 smoke particles emitted from CC. These differences can be explained by the fact that biomass
294 fuels generally contain large amounts of biopolymers, such as carbohydrates (cellulose,

295 hemicellulose, etc.); the burning of biomass fuels produces more highly polar compounds,
296 such as phenols, polyols, and polysaccharides; and CC emits more relatively hydrophobic and
297 less polar components, such as coal tar and polycyclic aromatic species (Wu et al., 2014; Wu
298 et al., 2021; Huang et al., 2020).

299

300 **3.2 Light absorption**

301 AAE and MAE₃₆₅ are important optical indicators of the light absorption properties of
302 atmospheric BrC and were investigated for BB- and CC-derived BrC in this study. As shown
303 in Figures 2a and c, the AAE values of the WSOC and HULIS-C fractions were 6.1–9.9
304 (mean 7.8 ± 1.6) and 7.2–9.6 (mean 8.5 ± 0.8), respectively, for BB smoke and 8.5–16 (mean
305 13 ± 2.9) and 10–16 (mean 14 ± 2.3), respectively, for CC smoke. These results were
306 comparable to those measured for combustion-emitted aerosols with reported AAE values for
307 HULIS of 7.4–8.3 (Park and Yu, 2016) and 6.2–8.1 (Fan et al., 2016, 2018) for BB smoke and
308 5.2–14 for CC smoke (Li et al., 2019). Moreover, the AAE values of BB WSOC and HULIS
309 were also comparable to those reported for WSOC in urban aerosols in Beijing (mean $7.28 \pm$
310 0.24) (Cheng et al., 2016), HULIS in Amazon BB aerosols (~ 7.10) (Hoffer et al., 2006),
311 urban aerosols in Beijing (5.3–5.8) (Yan et al., 2015), and aerosols in the Tibetan Plateau
312 (7.14–9.35) (Wu et al., 2020) but higher than that (1.2–5.4, mean of 3.2) of water-soluble BrC
313 in Los Angeles (Zhang et al., 2013). However, the AAE values of the water-soluble BrC
314 fraction from CC were almost higher than those in ambient aerosols, as described above. The
315 AAE values for MSOC were 5.62–6.95 for BB smoke and 8.46–10.0 for CC smoke. It was
316 obvious that the AAE value of BB MSOC was comparable to that of urban aerosols (average

317 7.10 ± 0.45) in Beijing (Cheng et al., 2016) and the reported value (5.0–6.5) for urban
318 aerosols in India (Mukherjee et al., 2020), but the AAE values of CC MSOC were likely
319 higher than those for urban aerosols. It is obvious that CC-derived BrC fractions (WSOC,
320 HULIS-C, and MSOC) generally have relatively higher AAE values than ambient BrC,
321 thereby suggesting that the contribution of CC may improve the AAE values of BrC in the
322 atmosphere and should not be ignored.

323 As shown in Figures 2a and c, the average AAE values of the WSOC, HULIS-C, and
324 MSOC fractions in BB smoke were all lower than those for the same BrC fraction in CC
325 smoke, indicating that BB-derived BrC had a weaker wavelength dependence than
326 CC-derived BrC. This finding agreed with the results reported in a previous study (Fan et al.,
327 2016). The AAE values of the BrC fraction also varied according to the type of BrC fraction.
328 HULIS-C had the highest AAE values, which were slightly higher than those for WSOC but
329 much higher than those for MSOC (Figures 2a and 2c), indicating that water-soluble BrC
330 fractions had a greater wavelength dependency than the corresponding MSOC. This was
331 similar to the results of previous studies that found higher AAE values for WSOC than
332 MSOC in ambient aerosols (Cheng et al., 2016; Kim et al., 2016) and can be explained by the
333 fact that the strongly light-absorbing organic molecules are generally comprised of aromatic
334 structures with a high degree of conjugation and low solubility in water.

335 MAE_{365} is an important parameter that characterizes the light absorption ability of
336 atmospheric BrC. As shown in Figures 2b and d, the MAE_{365} values of WSOC and HULIS-C
337 were 0.9–1.5 (mean 1.2 ± 0.3) and 1.1–1.6 (mean 1.3 ± 0.2) m^2/gC , respectively, for BB
338 smoke and 0.2–0.8 (mean 0.3 ± 0.2) and 0.3–1.1 (mean 0.4 ± 0.3) m^2/gC , respectively, for CC

339 smoke. As the hydrophobic fraction of WSOC, the MAE₃₆₅ values of HULIS-C in BB and CC
340 smoke were slightly higher than that of the corresponding WSOC, suggesting that HULIS-C
341 had a stronger light absorbing ability. Moreover, the MAE₃₆₅ values of WSOC and HULIS-C
342 in BB smoke were comparable with the results of previous studies of the WSOC and
343 HULIS-C fractions in combustion-released smokes and ambient aerosols. For example, the
344 reported MAE₃₆₅ values of WSOC and HULIS-C were 0.8–1.6 and 1.0–1.5 m²/gC,
345 respectively, in BB smoke PM_{2.5} (Park and Yu, 2016; Huo et al., 2018); 0.3–1.0 and 0.5–1.4
346 m²/gC, respectively, in CC smoke particles (Li et al., 2018); and 0.1–1.5 m²/gC in ambient
347 aerosols (Cheng et al., 2016; Yan et al., 2015; Zou et al., 2020). In contrast, the MAE₃₆₅
348 values for MSOC were 1.9–2.7 m²/gC for BB smoke and 1.0–2.7 m²/gC for CC smoke,
349 which were 1.3–8.5 times higher than the corresponding values for HULIS-C and WSOC and
350 suggest that MSOC had the strongest light absorption capacity. The MAE₃₆₅ values of BB and
351 CC MSOC were comparable to the MAE₃₆₅ values of urban aerosols in Beijing winter
352 (average 1.45 ± 0.26 m²/gC) (Yan et al., 2015) and the water-insoluble BrC (0.85–2.45 m²/gC)
353 in summer and winter ambient aerosols in Xi'an, Northwest China (Li et al., 2020b).
354 However, the values were higher than the MAE₃₆₅ value of aerosol MSOC in the Central
355 Tibetan Plateau (0.27–0.86 m²/gC) (Wu et al., 2020), which may be due to the relatively low
356 combustion source contribution in this region.

357 As shown in Figures 2b and d, some differences were observed among the BrC fractions.
358 WSOC, HULIS-C, and MSOC in BB smoke all had relatively higher MAE₃₆₅ values than the
359 same BrC fractions from CC, which suggested that BrC components emitted from BB had a
360 relatively higher light absorption ability than those from CC and may therefore have a higher

361 radiative force (Alexander et al., 2008). This finding is important for accurately assessing the
362 climate effects of BrC from different combustion sources.

363

364 **3.3. Spectral EEM features and identification of PARAFAC components**

365 **3.3.1. The EEM fluorescence properties**

366 Fluorescence spectroscopy is a highly sensitive analytical technique for the identification
367 of the sources and types of fluorophores in natural organic matter. In recent decades,
368 fluorescence spectroscopy has been widely used to characterize the fluorophores of
369 atmospheric BrC in field and laboratory studies (Chen et al., 2017; Chen et al., 2016; Qin et
370 al., 2018; Fan et al., 2020). The typical EEM spectra of WSOC, HULIS-C, and MSOC
371 fractions from BB and CC are shown in Figure S2. To avoid concentration effects, the
372 fluorescence spectra were normalized by the OC content of WSOC, HULIS-C, and MSOC;
373 and the specific fluorescence intensities (a.u. L/(gC)) are shown.

374 In general, the different regions in the fluorescence spectra can be associated with
375 organic fractions with different chemical characteristics (Table S1) (Chen et al., 2003; Cui et
376 al., 2016; Qin et al., 2018). As shown in Figure S2, the EEM spectra were divided into five
377 regions: protein-like amino acid (I), protein-like UV region (II, peak T₁), fulvic-like (III),
378 tryptophan-like or microbial byproducts (IV, peak T₂), and humic-like (V) fluorophores (Qin
379 et al., 2018; Cui et al., 2016; Chen et al., 2016). It was observed that the WSOC and
380 HULIS-C fractions exhibited two types of fluorescence peaks at $\lambda_{\text{ex}}/\lambda_{\text{em}} \approx (220\text{--}240)/(350\text{--}$
381 $390)$ nm (peak T₁) and $\lambda_{\text{ex}}/\lambda_{\text{em}} \approx (260\text{--}300)/(240\text{--}380)$ nm (peak T₂) (as marked in Figure S2),
382 which were mainly located in regions II and IV, respectively. These bands in the same range

383 as peaks T_1 and T_2 have previously been identified in the EEM fluorescence spectra of
384 water-soluble organic matter from rainwater/fog water (Santos et al., 2009; Santos et al., 2012)
385 and $PM_{2.5}$ in an industrial city in Northwest China (Qin et al., 2018). As shown in Figure S2,
386 the fluorescence peaks T_1 and/or T_2 were the dominant peaks for WSOC and HULIS-C in
387 BB- and CC-derived smoke samples, which were consistent with previous observations of the
388 WSOC and HULIS-C fractions from BB (Huo et al., 2018; Fan et al., 2020). In general, peak
389 T_1 mainly corresponded to the protein-like UV region, with a minor contribution from
390 fulvic-like substances; whereas peak T_2 was assigned as tryptophan-like or microbial
391 byproduct fluorophores. However, as reported in recent studies, non-nitrogen-containing
392 species, such as naphthalene and phenol-derived compounds, may also contribute to the
393 fluorophores with peak T_2 in atmospheric aerosols (Chen et al., 2017, 2020). In addition, the
394 intensity of peak T_1 for BB- and CC-derived HULIS-C fractions was clearly stronger than the
395 peak in ambient HULIS described in previous studies (Chen et al., 2017; Chen et al., 2016;
396 Fan et al., 2020; Qin et al., 2018), indicating that these BB- and CC-derived HULIS-C might
397 consist of more protein-like and/or aromatic amino acids than atmospheric HULIS.
398 However, these protein-like fluorescence peaks were observed to gradually decrease during
399 the aging process (e.g., hydroxyl radicals or ozone oxidation) in previous studies (Fan et al.,
400 2019, 2020). This implied that most protein-like fluorophores in BB or CC BrC fractions may
401 have high reactivity.

402 As shown in Figure S2, the EEM spectra of the three MSOC fractions from crop straw
403 burning all had a strong fluorescence peak at long emission wavelengths ($E_X = 205\text{--}280$ nm,
404 $E_M = 360\text{--}380$ nm), which were located in regions V and IV and were generally assigned to

405 humic-like fluorophores (Qin et al., 2018) or less oxygenated humic-like species (Chen et al.,
406 2017; Chen et al., 2016). This peak was very weak or unobservable in the EEM fluorescence
407 spectra of the WSOC and HULIS-C fractions, suggesting that the higher intensity of the
408 fluorescence peak was mainly due to water-insoluble organic compounds with a high degree
409 of conjugation and/or aromaticity. As shown in Figure S2, unlike the EEM spectra of crop
410 straw MSOC, the EEM spectra of the three types of wood branches all displayed two obvious
411 fluorescence peaks (e.g., peaks T₁ and T₂). These differences in the EEM spectra between
412 crop straw and wood burning-derived MSOC might be attributed to their molecular
413 differences, which should be investigated in future studies. The EEM spectra of the four
414 bituminous coal smoke MSOC fractions displayed a similar fluorescence peak T₂ in the EEM
415 spectra, but only a strong peak T₁ was observed in the anthracite coal smoke MSOC. These
416 differences indicate that the fluorophores of MSOC were significantly influenced by the type
417 of fuel.

418

419 **3.3.2. Identification of PARAFAC components**

420 PARAFAC analysis further determined the fluorescent components of the water-soluble
421 BrC fraction (WSOC and HULIS-C) and MSOC. As shown in Figure 3a, WSOC and
422 HULIS-C generally contained four types of fluorophores (C_{w1}–C_{w4}). Based on previous
423 studies of BrC EEM in combustion aerosols and ambient aerosols (Chen et al., 2017; Chen et
424 al., 2016; Huo et al., 2018; Qin et al., 2018), these four fluorophores could be assigned to two
425 protein-like substances (C_{w1} and C_{w2}), one polyphenol-like component (C_{w3}), and one
426 humic-like compound (C_{w4}). The E_x/E_m maximum of C_{w1} was located at 230/365 nm in

427 region II and was confirmed to be protein-like UV fluorophores. C_w2 (E_x = 270 nm, E_m =
428 350 nm) was placed in region IV and was determined to be tryptophan-like or microbial
429 byproduct compounds (Chen et al., 2016; Li et al., 2020a), which have been identified in
430 aerosol WSOM (Chen et al., 2016; Matos et al., 2015) and BB-derived primary and secondary
431 WSOM (Huo et al., 2018). C_w3 (E_x = 205/275 nm, E_m = 330 nm) was located in regions I
432 and IV and had the characteristics of aromatic protein-like fluorophores or polyphenol-like
433 components, most likely representing the fluorescence properties of polyphenol-like
434 components or compounds containing phenoxy groups (Mostofa et al., 2011). C_w4 (E_x =
435 215–320 nm, E_m = 415 nm) was located in the area where regions III and V overlap. These
436 overlapping peaks were assigned to strong humic-like species fluorescence with an excitation
437 wavelength = 245 nm and two weaker shoulder peaks (Chen et al., 2016; Li et al., 2020a; Qin
438 et al., 2018; Huo et al., 2018; Fan et al., 2020); therefore, C_w4 was associated with typical
439 humic-like fluorophores. In summary, the fluorescence components identified in the WSOC
440 and HULIS-C fractions suggested that protein-like and humic-like substances were the two
441 major backbone components in water-soluble BrC fractions.

442 As shown in Figure 3b, four independent fluorescence components were also identified
443 by PARAFAC analysis of MSOC (C_M1–C_M4). These components were similar to those of
444 WSOC and HULIS-C, especially the positioning of the main peaks of the four fluorescent
445 fluorophores. However, some small differences for component 2 (C_w2 and C_M2) and
446 component 4 (C_w4 and C_M4) fluorophores were also observed. Unlike C_w2 in WSOC and
447 HULIS-C, C_M2 in MSOC had its E_x/E_m maximum at 285/360 nm, which was assigned to
448 tryptophan-like compounds (Fan et al., 2020; Qin et al., 2018). In addition, two lower

449 intensities of peaks at a lower excitation wavelength were also detected. The position of this
450 fluorescence was closer to that of the typical tryptophan-like chromophores in aquatic DOM
451 (Murphy et al., 2010). C_{M4} in MSOC had a strong peak (EX = 255 nm, EM = 295 nm) but
452 without the shoulder peaks observed for C_{W4} in WSOC (Chen et al., 2016; Hou et al., 2018).

453 The relative contributions of individual chromophores identified by PARAFAC analysis
454 were calculated to express the relative contribution of each independent chromophore to the
455 overall fluorescence properties and are shown in Figure 4. The protein-like fluorescence
456 group (components 1 and 2), which were located at low emission wavelengths, dominated the
457 fluorophores of the BrC fractions in most BB and CC smoke samples. As shown in Figure 4,
458 the contributions of protein-like substances in WSOC, HULIS-C, and MSOC were 47%–80%,
459 44%–87%, and 42%–70% (except CS MSOC), respectively, which were higher than the
460 contributions of polyphenol-like or humic-like substances in the same BrC fraction. These
461 results are similar to the results reported for BrC from biomass combustion emissions in
462 previous studies (Huo et al., 2018; Fan et al., 2020). However, they were significantly
463 different from the EEM-PARAFAC properties of BrC in ambient aerosols, in which
464 component 4 was the most abundant chromophore (Chen et al., 2016; Li et al., 2020a).
465 However, component 4 accounted for only 13%–33% (except CS MSOC) and 3.8%–31% of
466 the BB and CC BrC fluorescence intensities, respectively, which were significantly lower
467 than those reported previously in ambient aerosols (30%–38%) (Li et al., 2020a). Moreover,
468 the contribution of polyphenol-like chromophores was 4.0%–39% and was comparable to that
469 of ambient aerosols (18%–26%) (Li et al., 2020a; Chen et al., 2016). It is obvious that the
470 four fluorescent components were all detected in the BrC fractions in combustion-derived

471 smokes and atmospheric aerosols; however, the protein-like compounds were the dominant
472 fluorophores in combustion-derived BrC whereas a relatively higher content of humic-like
473 fluorophores was identified in ambient aerosol BrC. These differences may be due to the
474 influence of various sources and atmospheric chemical processes on fluorophores (Li et al.,
475 2020a; Fan et al., 2020).

476 Furthermore, some differences were also observed among the BrC fractions derived
477 from different sources. As shown in Figure 4, the water-soluble BrC (WSOC and HULIS-C)
478 from wood burning had a relatively higher content of component 3 than the water-soluble
479 BrC from crop straw burning, which may be associated with the relatively large amount of
480 lignin components in wood materials. In addition, even though their maturity was very
481 different, there was no regular trend in the relative content of the fluorescent groups.

482

483 **3.4. ¹H-NMR spectroscopy**

484 ¹H-NMR is an important analytical tool for the investigation of the functional groups of
485 WSOC and HULIS in rural/urban aerosols (Fan et al., 2016; Zou et al., 2020) and rainwater
486 (Santos et al., 2009; Santos et al., 2012). The typical ¹H-NMR spectra of the WSOC,
487 HULIS-C, and MSOC fractions in smoke emitted from BB crop straw (e.g., WS) and CC
488 (e.g., B-1) are shown in Figure 5, and the ¹H-NMR spectra of other BB and CC BrC fractions
489 are shown in Figure S3. These BrC fractions had ¹H-NMR spectra similar to those derived
490 from atmospheric HULIS and/or WSOC in rainwater (Santos et al., 2009; Santos et al., 2012),
491 BB aerosols (Fan et al., 2016), and ambient aerosols in urban and rural regions (Zou et al.,
492 2020).

493 As shown in Figure 5, the $^1\text{H-NMR}$ spectra were mainly composed of several distinct
494 sharp peaks superimposed on an unresolved broad band. According to previous studies and
495 reference NMR spectra (Zou et al., 2020; Chalbot et al., 2014; Chalbot et al., 2016), these
496 sharp peaks can be ascribed to low molecular weight organic compounds, such as
497 levoglucosan ($\delta 3.52$, $\delta 3.67$, $\delta 4.08$, and $\delta 5.45$ ppm), glucose ($\delta 3.88$ – $\delta 3.91$ and $\delta 3.81$ – $\delta 3.85$
498 ppm), and fructose ($\delta 3.79$ – $\delta 3.84$ ppm) associated with BB emissions; phthalic acid ($\delta 7.45$ –
499 $\delta 7.47$ and $\delta 7.58$ ppm) and terephthalic acid ($\delta 8.01$ ppm) associated with anthropogenic
500 activity; and the CH_3 in trimethylamine ($\delta 2.71$ and $\delta 2.89$ ppm), dimethylamine ($\delta 2.72$ ppm),
501 and monomethylamine ($\delta 2.55$ ppm) coemitted with ammonia. The relatively few and/or weak
502 sharp peaks in the $^1\text{H-NMR}$ spectra of HULIS-C compared with those of WSOC may be the
503 result of low molecular weight organic compounds that have been removed from HULIS-C
504 through SPE isolation. In addition, all BB-derived WSOC had a high intensity of sharp peaks
505 associated with carbohydrates, such as levoglucosan, glucose, and fructose resonances, which
506 may be released from the thermal reactions of biopolymers, such as celluloses. As a
507 comparison, several peaks ($\delta 0.90$ and $\delta 1.35$ ppm) were observed in MSOC and were mainly
508 located in the aliphatic region. These peaks were weaker in WSOC and HULIS-C, suggesting
509 that more less polar aliphatic compounds were present in the MSOC fraction.

510 Despite some sharp peaks being identified, most of the signals in the $^1\text{H-NMR}$ spectra of
511 the BrC fractions presented a continuous unresolved distribution, suggesting that BrC consists
512 of a complex mixture of organic substances (Fan et al., 2016; Chalbot et al., 2014; Chalbot et
513 al., 2016). As shown in Figure 5, the functional groups of smoke BrC could be divided into
514 four representative categories: (1) R-H: aliphatic protons in alkyl chains (0.6–1.9 ppm),

515 including methyl (R-CH₃) protons, methylene (R-CH₂) protons, and methyne (R-CH) protons;
516 (2) H-C-C=: aliphatic protons bound to carbon atoms adjacent to unsaturated groups (1.9–3.2
517 ppm), including carbonyl (H-C-C=O) and imino (H-C-C=N) groups or aromatic rings; (3)
518 H-C-O: protons bound to oxygenated aliphatic carbons atoms in alcohols, polyols, ethers, and
519 esters (3.4–4.4 ppm), generally indicating that carbohydrates and ethers were present in
520 organic matter; and (4) Ar-H: protons bound to aromatic carbon atoms (6.5–8.5 ppm) (Fan et
521 al., 2016; Zou et al., 2020). The distribution of the four types of protons was obtained by
522 integrating the area of the observed ¹H-NMR bands for each sample and is shown in Table 2.
523 These functional groups were also observed in the ¹H-NMR spectra of HULIS in ambient
524 aerosols. In general, HULIS in ambient aerosols (Chalbot et al., 2014; Chalbot et al., 2016)
525 and rainwater (Santos et al., 2012) were characterized by the predominance of H-C (41%–
526 60%), moderate contents of H-C-C= (25%–34%) and H-C-O (4.0%–49%), and a lesser
527 contribution of Ar-H (2.0%–6.0%). However, it was obvious that the relative content of Ar-H
528 groups (18%–37%) in HULIS-C from both combustion processes (BB and CC) was higher
529 than the levels in ambient HULIS (Table 2), which suggests that BB- and CC-derived
530 HULIS-C contained more aromatic structures than ambient HULIS. This was consistent with
531 reports that more aromatic structures are observed in HULIS in colder season aerosol
532 particles in northern China, which may be related to the amount of residential coal and straw
533 combustion (Li et al., 2018; Sun et al., 2017).

534 As shown in Table 2, the relative contents of the four functional groups (i.e., R-H,
535 H-C-C=, H-C-O, and Ar-H) varied with the type of BrC. For example, BB WSOC was always
536 characterized by a relatively high level of oxygenated H-C-O groups and a relatively low

537 level of aliphatic R-H groups compared with the corresponding MSOC extracted with
538 methanol. As shown in Figure 5, several strong signals in aliphatic R-H were also identified
539 in MSOC, but they were weaker in the WSOC fraction. This was considered reasonable
540 because the less polar aliphatic compounds were difficult to dissolve in water but could be
541 extracted by methanol. As the hydrophobic fraction of WSOC, HULIS-C contained a
542 relatively higher content of the Ar-H group and a relatively lower content of the oxygenated
543 H-C-O group than the original WSOC for all BB and CC smoke samples. This was due to
544 most of the low molecular oxygenated compounds not being retained by the
545 hydrophilic-lipophilic balance cartridges and the enrichment of aromatic species (Fan et al.,
546 2016; Zou et al., 2020).

547 Some distinct differences in the distribution of functional groups were also observed
548 among the BrC fractions from BB and CC. As shown in Figure 5, several oxygenated
549 compounds (e.g., levoglucosan) were identified, with higher intensity signals in the BB
550 WSOC fraction, but they were weaker in the WSOC fraction from CC. The relative content of
551 the H-C-O group was in the range of 34%–54% for the six BB WSOCs, which was higher
552 than the values (9.0–34%) for the five CC WSOCs. These oxygenated aliphatic compounds
553 were mainly assigned to carbohydrates and polyols that may be caused by the degradation of
554 biomass polymers such as cellulose (Fan et al., 2012; Fan et al., 2016; Lin et al., 2016). In
555 contrast, the BrC fractions from CC indicated a relatively higher level of unsaturated
556 functional groups (Table 2). For example, there was a relatively higher content of Ar-H
557 (30%–37%) and H-C-C= (34%–40%) in the smoke HULIS-C from CC than from BB,
558 indicating that CC HULIS-C contained more unsaturated structures, such as aromatic

559 structures and unsaturated aliphatics (Wu et al., 2014; Dong et al., 2021; Huang et al., 2020).

560

561 **3.5 Oxidative potential**

562 The oxidative potential of the BB- and CC-derived BrC fractions (i.e., WSOC, HULIS-C,
563 and MSOC) was investigated through a DTT assay, and the results are shown in Table S2 and
564 Figure 6. The DTT_m value of WSOC ranged from 0.5 pmol/min/μg (B-3) to 7.4 pmol/min/μg
565 (CS) with a mean of 3.8 pmol/min/μg. These DTT_m values are comparable with those for the
566 water soluble fractions of BB, CC, and diesel soot (1.4±0.6, 2.1±2.3 and 1.1±0.4 pmol/min/μg)
567 (Li et al., 2019; Zhu et al., 2019) but were much lower than the ranges of 14–25 pmol/min/μg
568 in Los Angeles wildfire aerosol samples, 22–68 pmol/min/μg in Atlanta PM_{2.5} samples, and
569 0.13±0.10 nmol/min/μg in Beijing PM_{2.5} samples (Verma et al., 2012; Bates et al., 2019, Yu et
570 al., 2019). These results suggested that the water-soluble fraction from BB and CC in this
571 study had a weaker ROS generation capacity than ambient aerosols, which was likely due to
572 the differences in the chemical composition of water-soluble fractions in BB and CC smoke
573 particles and ambient aerosols (Lin and Yu, 2011; Dou et al., 2015; Wong et al., 2019; Lin and
574 Yu, 2019). In general, ambient aerosols contain various sources; and the contribution of other
575 sources, such as vehicle emissions or anthropogenic emissions, and transition metals (e.g., Fe,
576 Cu) could increase the ability of atmospheric water-soluble fractions to produce ROS species
577 (Ma et al., 2018; Li et al., 2019). In addition, because of the evaporative loss of non- or
578 less-DTT active semivolatile organic compounds, the DTT activities of BB-derived
579 water-soluble fractions were enhanced during the aging process (Wong et al., 2019).

580 The DTT_m values of BB- and CC-derived HULIS-C ranged from 0.5 pmol/min/μg (B-3)

581 to 5.5 pmol/min/ μ g (RS) with a mean of 2.3 pmol/min/ μ g. These values were lower than the
582 range (15–45 pmol/min/ μ g) previously reported for ambient HULIS measured with the same
583 DTT assay (Lin and Yu, 2011; Ma et al., 2018; Verma et al., 2012). As an important
584 component of WSOC, the DTT activity of HULIS-C accounted 63.1% \pm 15.5% (41.4%–90.6%)
585 for that of WSOC in the BB and CC samples. These values of $DDT_{m,HULIS}/DDT_{m,WSOC}$ were
586 always higher than the organic carbon contribution of HULIS-C to WSOC for the same
587 sample (Table 1), therefore indicating that hydrophobic HULIS-C was an important
588 redox-active fraction in the BB- and CC-derived WSOC compounds. This result was
589 comparable with the higher oxidative contribution (64%) of HULIS-C following water
590 extracts from ambient aerosols in Atlanta (Verma et al., 2012). As reviewed by Win et al.,
591 (2018), this phenomenon can be explained by the specific organic species and functional
592 groups with DTT activity in HULIS-C. As described in previous studies and in this study, the
593 hydrophobic organic fractions isolated by the SPE column are mainly comprised of aromatic
594 compounds (Sannigrahi et al., 2006; Fan et al., 2016; Huo et al., 2018). These compounds
595 most likely include some of the redox-active species such as nitro-PAHs and quinones (Verma
596 et al., 2012), which can catalyze the oxidation of cellular antioxidants and generate ROS
597 species (Verma et al., 2012; Lin and Yu, 2011). In addition, as the charge transfer intermediate,
598 the reversible redox sites in HULIS lead to continuous ROS production (Ma et al., 2018; Lin
599 and Yu, 2011).

600 The DDT_m values of MSOC were in the range of 3.1 pmol/min/ μ g (B-4) to 84
601 pmol/min/ μ g (RS). These values were comparable to those reported in previous studies
602 involving atmospheric aerosol methanol extracts (\sim 55 pmol/min/ μ g) (Verma et al., 2012). As

603 shown in Figure 6, the DTT_m values of MSOC were much higher than those of WSOC and
604 HULIS-C from the same smoke samples, which suggested that the water-insoluble
605 components possessed significant oxidative properties that are relevant in toxicological
606 studies (Verma et al., 2012). These results were consistent with the results of previous studies
607 showing that water-insoluble compounds made the largest contribution to the oxidative
608 potential (Verma et al., 2012; Verma et al., 2015).

609 The DTT_m values of the BrC fractions varied with the type of fuel. As shown in Table S2,
610 the DTT_m values of BB WSOC were 4.5–7.4 pmol/min/μg, which was significantly higher
611 than the range of 0.5–2.1 pmol/min/μg for CC WSOC. Similar results were also observed for
612 the HULIS and MSOC fractions (Figure 6). These results indicated that the BrC fractions
613 from BB had higher oxidative potential values than those from CC and therefore more readily
614 catalyzed the generation of ROS. Furthermore, no regular variations were observed for the
615 oxidative potential of water-soluble BrC (e.g., WSOC and HULIS-C) in BB or CC smoke
616 samples, but the MSOC in crop straw smoke had a much higher DTT_{mass} value than the
617 MSOC in smoke samples from wood burning and CC. These differences were associated with
618 the differences in the amounts of redox-active compounds in each BrC fraction. There is a
619 need for more studies to investigate the relationship between the molecular structures in BB
620 smoke BrC and their DTT activities.

621

622 **3.6 Correlation between oxidative potential and chemical compositions of BrCs**

623 The BrCs produced by the BB and CC processes generally have different oxidative
624 potentials. The oxidative potential values of water-soluble BrC (WSOC and HULIS-C) were

625 much lower than those in MSOC, and the BB BrC fractions had higher oxidative potential
626 values than CC BrC fractions. These results suggested that BrC from different sources
627 exhibited distinct redox properties (Lin and Yu, 2011). To elucidate the association of
628 chemical characteristics with the oxidative potential of BB and CC, principal component
629 analysis (PCA) and Pearson correlation coefficients were conducted. Because the optical and
630 chemical properties were all obtained based on organic matter rather than PM, the oxidative
631 potential value normalized by the organic carbon mass (DTT_{OC}) of each fraction was used
632 here to present DTT activities, as well as the capacity to produce ROS species. In addition,
633 considering the statistical significance and quantity, the WSOC, HULIS-C and MSOC data
634 were analyzed together.

635 The results are shown in Figure 7 and Table 3. It is obvious that DTT_{OC} showed a
636 positive loading for both principal component 1 (PC1) and principal component 2 (PC2), and
637 DTT_{OC} was grouped with fluorophores C4 and MAE₃₆₅. These results are also given by the
638 Pearson correlation coefficient analysis in which the DTT_{OC} values showed significant
639 positive correlations with the parameters MAE₃₆₅ (R=0.697, p<0.01) and C4 proportion
640 (R=0.560, p<0.01). These results suggested that fluorophore C4 and high light-absorbing
641 components may significantly contribute to the DDT activities of BrC compounds.

642 Moreover, a significant positive relationship was also observed for C4 and MAE₃₆₅
643 (R=0.531, p<0.01), which indicated that C4 may be the main substance leading to the light
644 absorption of BrC. As reported previously, MAE₃₆₅ is related to the aromatic structure of the
645 conjugated system (Andrade-Eiroa et al., 2013, Fan et al., 2018), and fluorophore C4 was
646 considered to be a highly oxygenated species containing more carbonyl and carboxyl groups

647 (Chen et al., 2016, Li et al., 2020a). Therefore, the C4 component may mainly comprise
648 chemical species with a conjugated system and highly oxygenated species, such as quinones
649 or aromatic acids, which were believed to be the key components for the enhancement of the
650 ability of BrC to produce ROS species (Lin and Yu, 2011, Jiang et al., 2016, Verma et al.,
651 2012). These results also explained that the water-soluble BrC fractions in BB and CC smoke
652 showed relatively lower DTT consumption rate than those in ambient aerosols, in which
653 distinctly higher contents of fluorophore C4 were observed in the water-soluble fraction
654 (Matos et al., 2015; Chen et al., 2016).

655 We note that a positive correlation was observed between DTT_{OC} and R-H and a
656 negative correlation was observed between DTT_{OC} and Ar-H; however, it is scientifically
657 unreasonable. The main reason is that 1H NMR spectroscopy only measures the
658 concentrations of nonexchangeable hydrogen functional groups in BrC compounds. Some
659 organic compounds not carrying nonexchangeable hydrogen atoms, such as carbonyl or
660 carboxylic groups in BrC, cannot be detected by 1H NMR (Chalbot and Kavouras 2014;
661 Paglione et al., 2014). However, some of these oxygenated functional groups likely have the
662 ability to catalyze the generation of ROS species (Lin and Yu, 2011; Verma et al., 2015). In
663 addition, the H/C ratios of different hydrogen functional groups (i.e., R-H, H-C-C=, H-C-O,
664 and Ar-H) are very different; thus, the relative abundances of hydrogen functional groups are
665 difficult to compare with the carbon functional groups in BrC compounds (Decesari et al.,
666 2007). Therefore, it is necessary that other NMR techniques such as solution-state ^{13}C NMR
667 and two-dimensional heteronuclear (1H - ^{13}C) NMR be used to explore the chemical functional
668 groups associated with the oxidative potential of BrC in future studies.

669

670 **4. Conclusions**

671 In this study, the primary BrC fractions (i.e., WSOC, HULIS-C, and MSOC) emitted
672 from BB and CC were comprehensively investigated to determine their content, light
673 absorption, fluorophores, chemical properties, and oxidative potential. The results indicated
674 that both BB and CC were important sources of atmospheric BrC. It was found that BB
675 generated more of the water-soluble BrC fraction whereas CC released more of the
676 methanol-soluble BrC fraction in smoke PM_{2.5}. The results also enhanced our understanding
677 of the optical characteristics, chemical composition, and oxidative potential of the water- and
678 methanol-soluble BrC fractions. The MSOC fraction had higher MAE₃₆₅ values than
679 HULIS-C and WSOC, suggesting that water-insoluble BrC possessed a stronger light
680 absorbing capacity. In addition, BB BrC generally had higher MAE₃₆₅ and lower AAE values
681 than the corresponding CC BrC fractions, suggesting that the former had a higher light
682 absorption capacity and weaker wavelength dependence. The EEM-PARAFAC analysis
683 identified two protein-like compounds, one polyphenol-like component, and one humic-like
684 compound for all BrC fractions, among which the protein-like compounds were the dominant
685 components. The ¹H NMR analysis showed that the BB and CC BrC fractions contained R-H,
686 H-C-C=, H-C-O, and Ar-H groups, among which WSOC and HULIS-C were always
687 characterized by more oxygenated H-C-O groups and fewer aliphatic R-H groups than MSOC.
688 In addition, water-soluble BB BrC contained more highly oxygenated groups, suggesting that
689 they may have a stronger influence on the binding of metals by organic aerosols. Our study
690 also indicated that MSOC had higher DTT_m values than WSOC and HULIS-C, suggesting a

691 higher ROS generation capacity. In addition, relatively higher oxidative contribution
692 (63.1%±15.5%) of HULIS-C in WSOC were observed for all BB and CC smoke samples,
693 highlighted that HULIS was a major contributor of ROS production in WSOC. The BB BrC
694 fractions generally had a higher oxidative potential than CC BrC, which may suggest that BB
695 BrC was more readily able to catalyze the generation of ROS and therefore lead to more
696 severe harm to human health. More importantly, the PCA and Pearson correlation analysis
697 indicated that highly oxygenated humic-like fluorophore C4 may be an important DTT active
698 substance in BrC.

699 It should be noted that the BB and CC BrC fractions would experience a series of
700 chemical reactions once they are emitted into the atmosphere, resulting in changes to their
701 optical properties and DTT activities. Thus, future studies should focus on the chemical,
702 optical, and oxidative potential characteristics of BrC during the aging processes with smoke
703 particles in the tropospheric environment (Fan et al., 2020; Wong et al., 2019).

704

705 **Data availability.** The research data can be accessed upon request to the corresponding
706 author (songjzh@gig.ac.cn).

707

708 **Author contributions.** J. Song and P. Peng designed the research together. T. Cao, M. Li, and
709 C. Zou conducted the combustion experiments. T. Cao, M. Li, and C Yu extracted and
710 analyzed the BrC fractions. T. Cao and J. Song wrote the paper. X. Fan, J Wang, Z Yu, and P.
711 Peng commented on and revised the paper.

712

713 **Competing interests.** The authors declare that they have no conflicts of interest.

714

715 **Acknowledgments.** This study was supported by the National Natural Science Foundation of
716 China (41977188 and 41673177), the State Key Laboratory of Organic Geochemistry,
717 GIGCAS (SKLOG2020-3), and Guangdong Foundation for Program of Science and
718 Technology Research (2019B121205006). We greatly appreciate the assistance of two
719 anonymous reviewers for the helpful comments that greatly improved the quality of this
720 manuscript.

721

722 **References**

723 Alexander, D. T. L., Crozier, P. A., and Anderson, J. R.: Brown carbon spheres in East Asian
724 outflow and their optical properties, *Science*, 321, 833-836, 10.1126/science.1155296,
725 2008.

726 Andrade-Eiroa, Á., Canle, M., and Cerdá, V.: Environmental Applications of
727 Excitation-Emission Spectrofluorimetry: An In-Depth Review I, *Applied Spectroscopy*
728 *Reviews*, 48, 1-49, 10.1080/05704928.2012.692104, 2013.

729 Andreae, M. O., and Gelencser, A.: Black carbon or brown carbon? The nature of
730 light-absorbing carbonaceous aerosols, *Atmospheric Chemistry and Physics*, 6,
731 3131-3148, DOI 10.5194/acp-6-3131-2006, 2006.

732 Atwi, K., Mondal, A., Pant, J., Cheng, Z., El Hajj, O., Ijeli, I., Handa, H., and Saleh, R.:
733 Physicochemical properties and cytotoxicity of brown carbon produced under different
734 combustion conditions, *Atmospheric Environment*, 244, 117881,

735 10.1016/j.atmosenv.2020.117881, 2021.

736 Bai, Z., Zhang, L., Cheng, Y., Zhang, W., Mao, J., Chen, H., Li, L., Wang, L., and Chen, J.:
737 Water/Methanol-Insoluble Brown Carbon Can Dominate Aerosol-Enhanced Light
738 Absorption in Port Cities, *Environmental science & technology*, 54, 14889-14898,
739 10.1021/acs.est.0c03844, 2020.

740

741 Bates, J. T., Fang, T., Verma, V., Zeng, L., Weber, R. J., Tolbert, P. E., Abrams, J. Y., Sarnat, S.
742 E., Klein, M., Mulholland, J. A., and Russell, A. G.: Review of Acellular Assays of
743 Ambient Particulate Matter Oxidative Potential: Methods and Relationships with
744 Composition, Sources, and Health Effects, *Environmental science & technology*, 53,
745 4003-4019, 10.1021/acs.est.8b03430, 2019.

746 Chalbot, M. G., Brown, J., Chitranshi, P., da Costa, G. G., Pollock, E. D., and Kavouras, I. G.:
747 Functional characterization of the water-soluble organic carbon of size-fractionated
748 aerosol in the southern Mississippi Valley, *Atmos Chem Phys*, 14, 6075-6088,
749 10.5194/acp-14-6075-2014, 2014.

750 Chalbot, M. C., and Kavouras, I. G.: Nuclear magnetic resonance spectroscopy for
751 determining the functional content of organic aerosols: a review, *Environmental*
752 *pollution*, 191, 232-249, 10.1016/j.envpol.2014.04.034, 2014.

753 Chalbot, M. G., Chitranshi, P., da Costa, G. G., Pollock, E., and Kavouras, I. G.:
754 Characterization of water-soluble organic matter in urban aerosol by (1)H-NMR
755 spectroscopy, *Atmos Environ* (1994), 128, 235-245, 10.1016/j.atmosenv.2015.12.067,
756 2016.

757 Chen, Q., Miyazaki, Y., Kawamura, K., Matsumoto, K., Coburn, S., Volkamer, R., Iwamoto,
758 Y., Kagami, S., Deng, Y., Ogawa, S., Ramasamy, S., Kato, S., Ida, A., Kajii, Y., and
759 Mochida, M.: Characterization of Chromophoric Water-Soluble Organic Matter in Urban,
760 Forest, and Marine Aerosols by HR-ToF-AMS Analysis and Excitation-Emission Matrix
761 Spectroscopy, *Environmental science & technology*, 50, 10351-10360,
762 10.1021/acs.est.6b01643, 2016.

763 Chen, Q., Ikemori, F., Nakamura, Y., Vodicka, P., Kawamura, K., and Mochida, M.: Structural
764 and Light-Absorption Characteristics of Complex Water-Insoluble Organic Mixtures in
765 Urban Submicrometer Aerosols, *Environmental science & technology*, 51, 8293-8303,
766 10.1021/acs.est.7b01630, 2017.

767 Chen, Q., Wang, M., Wang, Y., Zhang, L., Li, Y., and Han, Y.: Oxidative Potential of
768 Water-Soluble Matter Associated with Chromophoric Substances in PM_{2.5} over Xi'an,
769 China, *Environmental science & technology*, 53, 8574-8584, 10.1021/acs.est.9b01976,
770 2019.

771 Chen, Q., Li, J., Hua, X., Jiang, X., Mu, Z., Wang, M., Wang, J., Shan, M., Yang, X., Fan, X.,
772 Song, J., Wang, Y., Guan, D., and Du, L.: Identification of species and sources of
773 atmospheric chromophores by fluorescence excitation-emission matrix with parallel
774 factor analysis, *The Science of the total environment*, 718, 137322,
775 10.1016/j.scitotenv.2020.137322, 2020.

776 Chen, W., Westerhoff, P., Leenheer, J. A., and Booksh, K.: Fluorescence excitation - Emission
777 matrix regional integration to quantify spectra for dissolved organic matter,
778 *Environmental science & technology*, 37, 5701-5710, 10.1021/es034354c, 2003.

779 Chen, Y., and Bond, T. C.: Light absorption by organic carbon from wood combustion,
780 Atmospheric Chemistry and Physics, 10, 1773-1787, DOI 10.5194/acp-10-1773-2010,
781 2010.

782 Cheng, Y., He, K. B., Du, Z. Y., Engling, G., Liu, J. M., Ma, Y. L., Zheng, M., and Weber, R.
783 J.: The characteristics of brown carbon aerosol during winter in Beijing, Atmospheric
784 Environment, 127, 355-364, 10.1016/j.atmosenv.2015.12.035, 2016.

785 Cui, X., Zhou, D., Fan, W., Huo, M., Crittenden, J. C., Yu, Z., Ju, P., and Wang, Y.: The
786 effectiveness of coagulation for water reclamation from a wastewater treatment plant
787 that has a long hydraulic and sludge retention times: A case study, Chemosphere, 157,
788 224-231, 10.1016/j.chemosphere.2016.05.009, 2016.

789 Decesari, S., Mircea, M., Cavalli, F., Fuzzi, S., Moretti, F., Tagliavini, E., and Facchini, M. C.:
790 Source attribution of water-soluble organic aerosol by nuclear magnetic resonance
791 spectroscopy, Environmental science & technology, 41, 2479-2484, 10.1021/es0617111,
792 2007.

793 Dong, Z., Jiang, N., Zhang, R., Xu, Q., Ying, Q., Li, Q., and Li, S.: Molecular characteristics,
794 source contributions, and exposure risks of polycyclic aromatic hydrocarbons in the core
795 city of Central Plains Economic Region, China: Insights from the variation of haze
796 levels, The Science of the total environment, 757, 143885,
797 10.1016/j.scitotenv.2020.143885, 2021.

798 Dou, J., Lin, P., Kuang, B. Y., and Yu, J. Z.: Reactive Oxygen Species Production Mediated
799 by Humic-like Substances in Atmospheric Aerosols: Enhancement Effects by Pyridine,
800 Imidazole, and Their Derivatives, Environmental science & technology, 49, 6457-6465,

801 10.1021/es5059378, 2015.

802 Evangeliou, N., Kylling, A., Eckhardt, S., Myroniuk, V., Stebel, K., Paugam, R., Zibtsev, S.,
803 and Stohl, A.: Open fires in Greenland in summer 2017: transport, deposition and
804 radiative effects of BC, OC and BrC emissions, *Atmospheric Chemistry and Physics*, 19,
805 1393-1411, 10.5194/acp-19-1393-2019, 2019.

806 Fan, X., Li, M., Cao, T., Cheng, C., Li, F., Xie, Y., Wei, S., Song, J., and Peng, P. a.: Optical
807 properties and oxidative potential of water-and alkaline-soluble brown carbon in smoke
808 particles emitted from laboratory simulated biomass burning, *Atmospheric Environment*,
809 194, 48-57, 10.1016/j.atmosenv.2018.09.025, 2018.

810 Fan, X., Yu, X., Wang, Y., Xiao, X., Li, F., Xie, Y., Wei, S., Song, J., and Peng, P. a.: The
811 aging behaviors of chromophoric biomass burning brown carbon during dark aqueous
812 hydroxyl radical oxidation processes in laboratory studies, *Atmospheric Environment*,
813 205, 9-18, 10.1016/j.atmosenv.2019.02.039, 2019.

814 Fan, X., Cao, T., Yu, X., Wang, Y., Xiao, X., Li, F., Xie, Y., Ji, W., Song, J., Peng, P., amp,
815 apos, and an: The evolutionary behavior of chromophoric brown carbon during ozone
816 aging of fine particles from biomass burning, *Atmospheric Chemistry and Physics*, 20,
817 4593-4605, 10.5194/acp-20-4593-2020, 2020.

818 Fan, X. J., Song, J. Z., and Peng, P. A.: Comparison of isolation and quantification methods to
819 measure humic-like substances (HULIS) in atmospheric particles, *Atmospheric*
820 *Environment*, 60, 366-374, 10.1016/j.atmosenv.2012.06.063, 2012.

821 Fan, X. J., Wei, S. Y., Zhu, M. B., Song, J. Z., and Peng, P. A.: Comprehensive
822 characterization of humic-like substances in smoke PM_{2.5} emitted from the combustion

823 of biomass materials and fossil fuels, *Atmospheric Chemistry and Physics*, 16,
824 13321-13340, 10.5194/acp-16-13321-2016, 2016.

825 Gao, D., Mulholland, J. A., Russell, A. G., and Weber, R. J.: Characterization of
826 water-insoluble oxidative potential of PM_{2.5} using the dithiothreitol assay, *Atmospheric*
827 *Environment*, 224, 117327, 10.1016/j.atmosenv.2020.117327, 2020.

828 Geng, C., Chen, J., Yang, X., Ren, L., Yin, B., Liu, X., and Bai, Z.: Emission factors of
829 polycyclic aromatic hydrocarbons from domestic coal combustion in China, *Journal of*
830 *environmental sciences*, 26, 160-166, 10.1016/s1001-0742(13)60393-9, 2014.

831 Hakimzadeh, M., Soleimanian, E., Mousavi, A., Borgini, A., De Marco, C., Ruprecht, A. A.,
832 and Sioutas, C.: The impact of biomass burning on the oxidative potential of PM_{2.5} in
833 the metropolitan area of Milan, *Atmospheric Environment*, 224, 117328,
834 10.1016/j.atmosenv.2020.117328, 2020.

835 He, W., and Hur, J.: Conservative behavior of fluorescence EEM-PARAFAC components in
836 resin fractionation processes and its applicability for characterizing dissolved organic
837 matter, *Water research*, 83, 217-226, 10.1016/j.watres.2015.06.044, 2015.

838 Hoffer, A., Gelencser, A., Guyon, P., Kiss, G., Schmid, O., Frank, G. P., Artaxo, P., and
839 Andreae, M. O.: Optical properties of humic-like substances (HULIS) in
840 biomass-burning aerosols, *Atmospheric Chemistry and Physics*, 6, 3563-3570, DOI
841 10.5194/acp-6-3563-2006, 2006.

842 Hou, C., Shao, L., Hu, W., Zhang, D., Zhao, C., Xing, J., Huang, X., and Hu, M.:
843 Characteristics and aging of traffic-derived particles in a highway tunnel at a coastal city
844 in southern China, *The Science of the total environment*, 619-620, 1385-1393,

845 10.1016/j.scitotenv.2017.11.165, 2018.

846 Huang, R. J., Yang, L., Shen, J., Yuan, W., Gong, Y., Guo, J., Cao, W., Duan, J., Ni, H., Zhu,
847 C., Dai, W., Li, Y., Chen, Y., Chen, Q., Wu, Y., Zhang, R., Dusek, U., O'Dowd, C., and
848 Hoffmann, T.: Water-Insoluble Organics Dominate Brown Carbon in Wintertime Urban
849 Aerosol of China: Chemical Characteristics and Optical Properties, *Environmental*
850 *science & technology*, 54, 7836-7847, 10.1021/acs.est.0c01149, 2020.

851 Huo, Y. Q., Li, M., Jiang, M. H., and Qi, W. M.: Light absorption properties of HULIS in
852 primary particulate matter produced by crop straw combustion under different moisture
853 contents and stacking modes, *Atmospheric Environment*, 191, 490-499,
854 10.1016/j.atmosenv.2018.08.038, 2018.

855 Izhar, S., Gupta, T., and Panday, A. K.: Improved method to apportion optical absorption by
856 black and brown carbon under the influence of haze and fog at Lumbini, Nepal, on the
857 Indo-Gangetic Plains, *Environmental pollution*, 263, 114640,
858 10.1016/j.envpol.2020.114640, 2020.

859 Jiang, H., Jang, M., Sabo-Attwood, T., and Robinson, S. E.: Oxidative potential of secondary
860 organic aerosols produced from photooxidation of different hydrocarbons using outdoor
861 chamber under ambient sunlight, *Atmospheric Environment*, 131, 382-389,
862 10.1016/j.atmosenv.2016.02.016, 2016.

863 Kim, H., Kim, J. Y., Jin, H. C., Lee, J. Y., and Lee, S. P.: Seasonal variations in the
864 light-absorbing properties of water-soluble and insoluble organic aerosols in Seoul,
865 Korea, *Atmospheric Environment*, 129, 234-242, 10.1016/j.atmosenv.2016.01.042, 2016.

866 Kramer, A. J., Rattanavaraha, W., Zhang, Z., Gold, A., Surratt, J. D., and Lin, Y.-H.: Assessing

867 the oxidative potential of isoprene-derived epoxides and secondary organic aerosol,
868 Atmospheric Environment, 130, 211-218, 10.1016/j.atmosenv.2015.10.018, 2016.

869 Kumar, N. K., Corbin, J. C., Bruns, E. A., Massabo, D., Slowik, J. G., Drinovec, L., Mocnik,
870 G., Prati, P., Vlachou, A., Baltensperger, U., Gysel, M., El-Haddad, I., and Prevot, A. S.
871 H.: Production of particulate brown carbon during atmospheric aging of residential
872 wood-burning emissions, Atmospheric Chemistry and Physics, 18, 17843-17861,
873 10.5194/acp-18-17843-2018, 2018a.

874 Kumar, V., Rajput, P., and Goel, A.: Atmospheric abundance of HULIS during wintertime in
875 Indo-Gangetic Plain: impact of biomass burning emissions, Journal of Atmospheric
876 Chemistry, 75, 385-398, 10.1007/s10874-018-9381-4, 2018b.

877 Laskin, A., Laskin, J., and Nizkorodov, S. A.: Chemistry of atmospheric brown carbon,
878 Chemical reviews, 115, 4335-4382, 10.1021/cr5006167, 2015.

879 Lawaetz, A. J., and Stedmon, C. A.: Fluorescence Intensity Calibration Using the Raman
880 Scatter Peak of Water, Applied Spectroscopy, 63, 936-940,
881 10.1366/000370209788964548, 2009.

882 Li, J., Chen, Q., Hua, X., Chang, T., and Wang, Y.: Occurrence and sources of chromophoric
883 organic carbon in fine particulate matter over Xi'an, China, The Science of the total
884 environment, 725, 138290, 10.1016/j.scitotenv.2020.138290, 2020a.

885 Li, J., Zhang, Q., Wang, G., Li, J., Wu, C., Liu, L., Wang, J., Jiang, W., Li, L., Ho, K. F., and
886 Cao, J.: Optical properties and molecular compositions of water-soluble and
887 water-insoluble brown carbon (BrC) aerosols in northwest China, Atmospheric
888 Chemistry and Physics, 20, 4889-4904, 10.5194/acp-20-4889-2020, 2020b.

889 Li, M., Fan, X., Zhu, M., Zou, C., Song, J., Wei, S., Jia, W., and Peng, P.: Abundances and
890 light absorption properties of brown carbon emitted from residential coal combustion in
891 China, *Environmental science & technology*, 10.1021/acs.est.8b05630, 2019.

892 Li, R., Han, Y., Wang, L., Shang, Y., and Chen, Y.: Differences in oxidative potential of black
893 carbon from three combustion emission sources in China, *Journal of environmental
894 management*, 240, 57-65, 10.1016/j.jenvman.2019.03.070, 2019.

895 Li, X., Han, J., Hopke, P. K., Hu, J., Shu, Q., Chang, Q., and Ying, Q.: Quantifying primary
896 and secondary humic-like substances in urban aerosol based on emission source
897 characterization and a source-oriented air quality model, *Atmospheric Chemistry and
898 Physics*, 19, 2327-2341, 10.5194/acp-19-2327-2019, 2019.

899 Lin, M., and Yu, J. Z.: Dithiothreitol (DTT) concentration effect and its implications on the
900 applicability of DTT assay to evaluate the oxidative potential of atmospheric aerosol
901 samples, *Environmental pollution*, 251, 938-944, 10.1016/j.envpol.2019.05.074, 2019.

902 Lin, P., and Yu, J. Z.: Generation of reactive oxygen species mediated by humic-like
903 substances in atmospheric aerosols, *Environmental science & technology*, 45,
904 10362-10368, 10.1021/es2028229, 2011.

905 Lin, P., Laskin, J., Nizkorodov, S. A., and Laskin, A.: Revealing Brown Carbon
906 Chromophores Produced in Reactions of Methylglyoxal with Ammonium Sulfate,
907 *Environmental science & technology*, 49, 14257-14266, 10.1021/acs.est.5b03608, 2015.

908 Lin, P., Aiona, P. K., Li, Y., Shiraiwa, M., Laskin, J., Nizkorodov, S. A., and Laskin, A.:
909 Molecular Characterization of Brown Carbon in Biomass Burning Aerosol Particles,
910 *Environmental science & technology*, 50, 11815-11824, 10.1021/acs.est.6b03024, 2016.

911 Ma, Y., Cheng, Y., Qiu, X., Cao, G., Fang, Y., Wang, J., Zhu, T., Yu, J., and Hu, D.: Sources
912 and oxidative potential of water-soluble humic-like substances (HULIS_{WS}) in fine
913 particulate matter (PM_{2.5}) in Beijing, *Atmospheric Chemistry and Physics*, 18,
914 5607-5617, 10.5194/acp-18-5607-2018, 2018.

915 Matos, J. T. V., Freire, S. M. S. C., Duarte, R. M. B. O., and Duarte, A. C.: Natural organic
916 matter in urban aerosols: Comparison between water and alkaline soluble components
917 using excitation-emission matrix fluorescence spectroscopy and multiway data analysis,
918 *Atmospheric Environment*, 102, 1-10, 10.1016/j.atmosenv.2014.11.042, 2015.

919 Mostofa, K. M. G., Wu, F. C., Liu, C. Q., Vione, D., Yoshioka, T., Sakugawa, H., and Tanoue,
920 E.: Photochemical, microbial and metal complexation behavior of fluorescent dissolved
921 organic matter in the aquatic environments, *Geochem. J.*, 45, 235-254, 2011.

922 Moufarrej, L., Courcot, D., and Ledoux, F.: Assessment of the PM_{2.5} oxidative potential in a
923 coastal industrial city in Northern France: Relationships with chemical composition,
924 local emissions and long range sources, *The Science of the total environment*, 748,
925 141448, 10.1016/j.scitotenv.2020.141448, 2020.

926 Mukherjee, A., Dey, S., Rana, A., Jia, S., Banerjee, S., and Sarkar, S.: Sources and
927 atmospheric processing of brown carbon and HULIS in the Indo-Gangetic Plain: Insights
928 from compositional analysis, *Environmental pollution*, 267, 115440,
929 10.1016/j.envpol.2020.115440, 2020.

930 Murphy, K. R., Butler, K. D., Spencer, R. G. M., Stedmon, C. A., Boehme, J. R., and Aiken,
931 G. R.: Measurement of Dissolved Organic Matter Fluorescence in Aquatic Environments:
932 An Interlaboratory Comparison, *Environmental science & technology*, 44, 9405-9412,

933 10.1021/es102362t, 2010.

934 Murphy, K. R., Hambly, A., Singh, S., Henderson, R. K., Baker, A., Stuetz, R., and Khan, S.
935 J.: Organic matter fluorescence in municipal water recycling schemes: toward a unified
936 PARAFAC model, *Environmental science & technology*, 45, 2909-2916,
937 10.1021/es103015e, 2011.

938 Murphy, K. R., Stedmon, C. A., Graeber, D., and Bro, R.: Fluorescence spectroscopy and
939 multi-way techniques. *PARAFAC, Analytical Methods*, 5, 6557, 10.1039/c3ay41160e,
940 2013.

941 Nozière, B., González, N. J. D., Borg-Karlson, A.-K., Pei, Y., Redeby, J. P., Krejci, R.,
942 Dommen, J., Prevot, A. S. H., and Anthonsen, T.: Atmospheric chemistry in stereo: A
943 new look at secondary organic aerosols from isoprene, *Geophysical Research Letters*, 38,
944 n/a-n/a, 10.1029/2011gl047323, 2011.

945 Paglione, M., Saarikoski, S., Carbone, S., Hillamo, R., Facchini, M. C., Finessi, E.,
946 Giulianelli, L., Carbone, C., Fuzzi, S., Moretti, F., Tagliavini, E., Swietlicki, E., Eriksson
947 Stenström, K., Prévôt, A. S. H., Massoli, P., Canaragatna, M., Worsnop, D., and Decesari,
948 S.: Primary and secondary biomass burning aerosols determined by proton nuclear
949 magnetic resonance ($^1\text{H-NMR}$) spectroscopy during the 2008
950 EUCAARI campaign in the Po Valley (Italy), *Atmospheric Chemistry and Physics*, 14,
951 5089-5110, 10.5194/acp-14-5089-2014, 2014.

952 Park, S.-S., Sim, S. Y., Bae, M.-S., and Schauer, J. J.: Size distribution of water-soluble
953 components in particulate matter emitted from biomass burning, *Atmospheric
954 Environment*, 73, 62-72, 10.1016/j.atmosenv.2013.03.025, 2013.

955 Park, S. S., and Yu, J.: Chemical and light absorption properties of humic-like substances
956 from biomass burning emissions under controlled combustion experiments, *Atmospheric*
957 *Environment*, 136, 114-122, 10.1016/j.atmosenv.2016.04.022, 2016.

958 Pietrogrande, M. C., Bertoli, I., Clauser, G., Dalpiaz, C., Dell'Anna, R., Lazzeri, P., Lenzi, W.,
959 and Russo, M.: Chemical composition and oxidative potential of atmospheric particles
960 heavily impacted by residential wood burning in the alpine region of northern Italy,
961 *Atmospheric Environment*, 253, 118360, 10.1016/j.atmosenv.2021.118360, 2021.

962 Qin, J., Zhang, L., Zhou, X., Duan, J., Mu, S., Xiao, K., Hu, J., and Tan, J.: Fluorescence
963 fingerprinting properties for exploring water-soluble organic compounds in PM 2.5 in an
964 industrial city of northwest China, *Atmospheric Environment*, 184, 203-211,
965 10.1016/j.atmosenv.2018.04.049, 2018.

966 Sannigrahi, P., Sullivan, A. P., Weber, R. J., and Ingall, E. D.: Characterization of
967 water-soluble organic carbon in urban atmospheric aerosols using solid-state C-13 NMR
968 spectroscopy, *Environmental science & technology*, 40, 666-672, 10.1021/es051150i,
969 2006.

970 Santos, P. S., Otero, M., Duarte, R. M., and Duarte, A. C.: Spectroscopic characterization of
971 dissolved organic matter isolated from rainwater, *Chemosphere*, 74, 1053-1061,
972 10.1016/j.chemosphere.2008.10.061, 2009.

973 Santos, P. S., Santos, E. B., and Duarte, A. C.: First spectroscopic study on the structural
974 features of dissolved organic matter isolated from rainwater in different seasons, *The*
975 *Science of the total environment*, 426, 172-179, 10.1016/j.scitotenv.2012.03.023, 2012.

976 Seo, I., Lee, K., Bae, M. S., Park, M., Maskey, S., Seo, A., Borlaza, L. J. S., Cosep, E. M. R.,

977 and Park, K.: Comparison of physical and chemical characteristics and oxidative
978 potential of fine particles emitted from rice straw and pine stem burning, *Environmental*
979 *pollution*, 267, 115599, 10.1016/j.envpol.2020.115599, 2020.

980 Shen, G., Chen, Y., Wei, S., Fu, X., Zhu, Y., and Tao, S.: Mass absorption efficiency of
981 elemental carbon for source samples from residential biomass and coal combustions,
982 *Atmospheric Environment*, 79, 79-84, 10.1016/j.atmosenv.2013.05.082, 2013.

983 Singh, G. K., Choudhary, V., Rajeev, P., Paul, D., and Gupta, T.: Understanding the origin of
984 carbonaceous aerosols during periods of extensive biomass burning in northern India,
985 *Environmental pollution*, 270, 116082, 10.1016/j.envpol.2020.116082, 2021.

986 Sun, J., Zhi, G., Hitznerberger, R., Chen, Y., Tian, C., Zhang, Y., Feng, Y., Cheng, M., Zhang,
987 Y., Cai, J., Chen, F., Qiu, Y., Jiang, Z., Li, J., Zhang, G., and Mo, Y.: Emission factors
988 and light absorption properties of brown carbon from household coal combustion in
989 China, *Atmospheric Chemistry and Physics*, 17, 4769-4780, 10.5194/acp-17-4769-2017,
990 2017.

991 van der Werf, G. R., Randerson, J. T., Giglio, L., Collatz, G. J., Mu, M., Kasibhatla, P. S.,
992 Morton, D. C., DeFries, R. S., Jin, Y., and van Leeuwen, T. T.: Global fire emissions and
993 the contribution of deforestation, savanna, forest, agricultural, and peat fires (1997-2009),
994 *Atmospheric Chemistry and Physics*, 10, 11707-11735, 10.5194/acp-10-11707-2010,
995 2010.

996 Verma, V., Rico-Martinez, R., Kotra, N., King, L., Liu, J., Snell, T. W., and Weber, R. J.:
997 Contribution of water-soluble and insoluble components and their
998 hydrophobic/hydrophilic subfractions to the reactive oxygen species-generating potential

999 of fine ambient aerosols, *Environmental science & technology*, 46, 11384-11392,
1000 10.1021/es302484r, 2012.

1001 Verma, V., Fang, T., Guo, H., King, L., Bates, J. T., Peltier, R. E., Edgerton, E., Russell, A. G.,
1002 and Weber, R. J.: Reactive oxygen species associated with water-soluble
1003 PM_{2.5} in the southeastern United States: spatiotemporal trends
1004 and source apportionment, *Atmospheric Chemistry and Physics*, 14, 12915-12930,
1005 10.5194/acp-14-12915-2014, 2014.

1006 Verma, V., Wang, Y., El-Afifi, R., Fang, T., Rowland, J., Russell, A. G., and Weber, R. J.:
1007 Fractionating ambient humic-like substances (HULIS) for their reactive oxygen species
1008 activity – Assessing the importance of quinones and atmospheric aging, *Atmospheric*
1009 *Environment*, 120, 351-359, 10.1016/j.atmosenv.2015.09.010, 2015.

1010 Win, M. S., Tian, Z., Zhao, H., Xiao, K., Peng, J., Shang, Y., Wu, M., Xiu, G., Lu, S.,
1011 Yonemochi, S., and Wang, Q.: Atmospheric HULIS and its ability to mediate the reactive
1012 oxygen species (ROS): A review, *Journal of environmental sciences*, 71, 13-31,
1013 10.1016/j.jes.2017.12.004, 2018.

1014 Wong, J. P. S., Tsagkaraki, M., Tsiotra, I., Mihalopoulos, N., Violaki, K., Kanakidou, M.,
1015 Sciare, J., Nenes, A., and Weber, R. J.: Effects of Atmospheric Processing on the
1016 Oxidative Potential of Biomass Burning Organic Aerosols, *Environmental science &*
1017 *technology*, 53, 6747-6756, 10.1021/acs.est.9b01034, 2019.

1018 Wu, D., Wang, Z., Chen, J., Kong, S., Fu, X., Deng, H., Shao, G., and Wu, G.: Polycyclic
1019 aromatic hydrocarbons (PAHs) in atmospheric PM_{2.5} and PM₁₀ at a coal-based
1020 industrial city: Implication for PAH control at industrial agglomeration regions, China,

1021 Atmospheric Research, 149, 217-229, 10.1016/j.atmosres.2014.06.012, 2014.

1022 Wu, G., Wan, X., Ram, K., Li, P., Liu, B., Yin, Y., Fu, P., Loewen, M., Gao, S., Kang, S.,
1023 Kawamura, K., Wang, Y., and Cong, Z.: Light absorption, fluorescence properties and
1024 sources of brown carbon aerosols in the Southeast Tibetan Plateau, Environmental
1025 pollution, 257, 113616, 10.1016/j.envpol.2019.113616, 2020.

1026 Wu, X., Liu, W., Gao, H., Alfaro, D., Sun, S., Lei, R., Jia, T., and Zheng, M.: Coordinated
1027 effects of air pollution control devices on PAH emissions in coal-fired power plants and
1028 industrial boilers, The Science of the total environment, 756, 144063,
1029 10.1016/j.scitotenv.2020.144063, 2021.

1030 Yan, C., Zheng, M., Sullivan, A. P., Bosch, C., Desyaterik, Y., Andersson, A., Li, X., Guo, X.,
1031 Zhou, T., Gustafsson, Ö., and Collett, J. L.: Chemical characteristics and light-absorbing
1032 property of water-soluble organic carbon in Beijing: Biomass burning contributions,
1033 Atmospheric Environment, 121, 4-12, 10.1016/j.atmosenv.2015.05.005, 2015.

1034 Yu, S., Liu, W., Xu, Y., Yi, K., Zhou, M., Tao, S., and Liu, W.: Characteristics and oxidative
1035 potential of atmospheric PM_{2.5} in Beijing: Source apportionment and seasonal variation,
1036 The Science of the total environment, 650, 277-287, 10.1016/j.scitotenv.2018.09.021,
1037 2019.

1038 Zhang, X., Lin, Y. H., Surratt, J. D., and Weber, R. J.: Sources, composition and absorption
1039 Angstrom exponent of light-absorbing organic components in aerosol extracts from the
1040 Los Angeles Basin, Environmental science & technology, 47, 3685-3693,
1041 10.1021/es305047b, 2013.

1042 Zhu, J., Chen, Y., Shang, J., and Zhu, T.: Effects of air/fuel ratio and ozone aging on

1043 physicochemical properties and oxidative potential of soot particles, *Chemosphere*, 220,
1044 883-891, 10.1016/j.chemosphere.2018.12.107, 2019.

1045 Zou, C., Li, M., Cao, T., Zhu, M., Fan, X., Peng, S., Song, J., Jiang, B., Jia, W., Yu, C., Song,
1046 H., Yu, Z., Li, J., Zhang, G., and Peng, P. a.: Comparison of solid phase extraction
1047 methods for the measurement of humic-like substances (HULIS) in atmospheric
1048 particles, *Atmospheric Environment*, 225, 117370, 10.1016/j.atmosenv.2020.117370,
1049 2020.

1050

1051 **Table 1.** The contributions of BrC fraction (WSOC, HULIS, and MSOC) in smoke samples (%).

Contents (%)	Biomass burning						Coal combustion				
	WS	RS	CS	PW	CR	WP	B-1	B-2	B-3	B-4	AN
OC	44±5.6	41±12	24±6.4	19±3.8	26±8.7	23±13	61±5.4	64±11	68±7.6	69±6.9	9.5±5.0
EC	2.5±0.9	1.3±0.6	4.4±2.8	10±3.4	5.0±3.3	13±7.6	0.2±0.1	1.1±0.8	0.3±0.1	0.8±0.6	0.1±0.0
TC ^a	46±5.5	42±12	28±8.2	29±4.0	32±9.6	36±19	61±5.4	65±11	69±6.7	69±6.8	9.5±5.0
WSOC/PM ^b	11±2.7	12±1.6	9.7±0.2	3.9±1.1	7.6±0.3	2.9±0.7	15±0.4	22±4.1	9.2±1.5	4.7±0.4	2.3±1.1
HULIS-C/PM ^b	6.7±1.3	7.8±0.2	4.0±0.5	1.7±0.3	3.1±0.6	1.0±0.4	6.0±0.6	10±0.8	4.2±0.4	2.0±0.2	0.5±0.1
MSOC/PM ^b	40±0.9	47±0.8	20±1.4	12±1.2	15±0.9	6.4±0.7	57±5.4	73±2.9	65±6.8	71±0.7	9.4±5.7
WSOC/TC ^c	22±6.0	23±3.0	25±3.0	14±3.1	32±3.0	21±9.4	25±2.9	29±4.3	14±3.2	6.4±0.5	22±8.5
HULIS-C/TC ^c	14±2.8	14±0.4	11±2.7	5.9±0.8	13±1.6	9.8±1.1	10±0.3	13±1.7	6.3±0.9	2.8±0.3	6.9±2.9
MSOC/TC ^c	82±2.2	88±1.5	57±11	53±7.5	78±16	52±27	99±0.2	95±1.9	98±0.1	96±0.1	95±1.8
HULIS-C/WSOC ^c	64±6.9	65±8.0	42±6.2	43±5.4	41±6.6	32±6.3	41±4.9	46±9.4	46±9.6	43±6.0	33±7.8
WSOC/OC ^c	23±5.9	23±3.1	33±0.9	24±4.0	36±2.6	35±3.2	25±2.9	30±4.5	14±3.3	6.4±0.5	26±3.9
HULIS-C/OC ^c	15±2.9	15±0.4	14±1.7	10±0.7	15±1.9	11±3.2	10±0.3	13±1.6	6.4±0.9	2.8±0.3	6.9±3.0
MSOC/OC ^c	88±1.9	91±1.2	70±4.5	76±2.5	72±6.7	77±4.5	99±0.1	96±0.5	98±0.1	98±0.5	96±1.6

1052 ^a Total Carbon: sum of OC and EC

1053 ^b The ratios of the mass of carbon (µgC) to the mass of PM (µg) for each sample.

1054 ^c The ratios of the mass of carbon (µgC) to the mass of carbon (µgC) for each sample.

1055

1056

1057

1058 **Table 2.** The proton species in the BrC fractions (WSOC, HULIS, and MSOC) of smoke samples.

Samples		WSOC				HULIS				MSOC			
		R-H	H-C-C=	H-C-O	Ar-H	R-H	H-C-C=	H-C-O	Ar-H	R-H	H-C-C=	H-C-O	Ar-H
		0.6-2.0 ^a	2.0-3.2	3.4-4.4	6.5-8.5	0.6-2.0	2.0-3.2	3.4-4.4	6.5-8.5	0.6-2.0	2.0-3.2	3.4-4.4	6.5-8.5
Biomass burning	WS	16 ^b	27	42	14	19	32	21	27	44	26	16	14
	RS	24	27	34	14	26	31	14	29	46	30	13	11
	CS	15	22	46	17	18	28	31	24	47	29	15	9
	PW	14	22	48	17	15	25	42	18	40	30	19	11
	CF	11	17	54	18	14	26	36	23	41	28	18	13
	WP	12	22	48	19	14	21	31	34	44	29	17	10
Coal combustion	B-1	18	41	9.0	32	17	40	5.0	37	40	28	2.0	30
	B-2	17	35	22	25	26	39	5.0	30	33	30	3.0	33
	B-3	17	39	14	30	22	34	8.0	35	34	30	2.0	33
	B-4	13	27	34	25	20	36	13	30	32	27	3.0	39
	AN	15	33	20	32	18	37	12	33	38	28	2.0	32

1059 ^a chemical shift: ppm. ^b percentage of each type of protons (%).

1060

1061

1062

1063 **Table 3.** Pearson correlation coefficient analysis between oxidation potential and chemical characteristics of BrC

	DTT _{OC} ^a	
	R	p
MAE ₃₆₅	0.697**	0.000
Fluorescence component 1 (%) ^b	-0.078	0.668
Fluorescence component 2 (%) ^b	-0.330	0.061
Fluorescence component 3 (%) ^b	0.151	0.402
Fluorescence component 4 (%) ^b	0.560**	0.001
R-H (%)	0.697**	0.000
H-C=C (%)	-0.247	0.166
H-C-O (%)	-0.223	0.213
Ar-H (%)	-0.345*	0.049

1064 a: DTT_{OC} were calculated using the DTT consumption rate divided by the mass of organic carbon.

1065 b: fluorescence component 1-4 present fluorophores 1-4 (C_w1-4 and C_M1-4) identified by PARAFAC method

1066 ** There was significant correlation in 99% confidence interval (bilateral) (p value no more than 0.01).

1067 * There was significant correlation in 95% confidence interval (bilateral) (p value no more than 0.05).

1068

1069

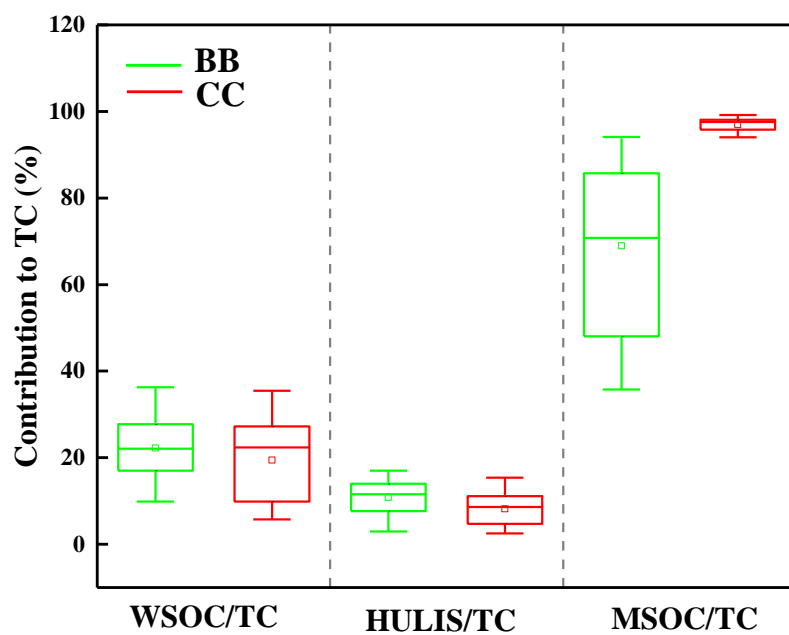


Figure 1. The abundances of BrC fraction in the smoke samples from biomass burning (BB) and coal combustion (CC)

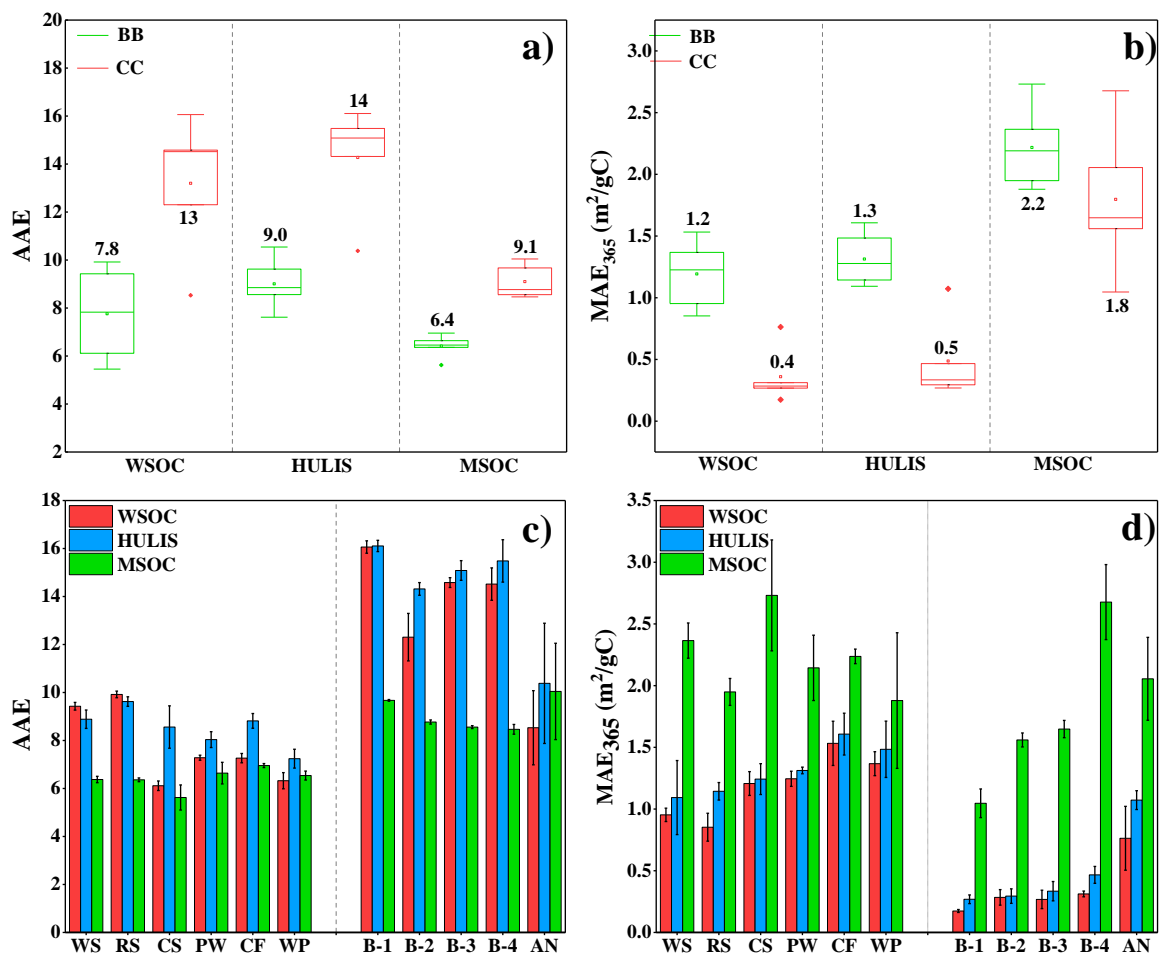


Figure 2. The AAE and MAE₃₆₅ values of WSOC, HULIS, and MSOC in smoke samples from biomass burning (BB) and coal combustion (CC)

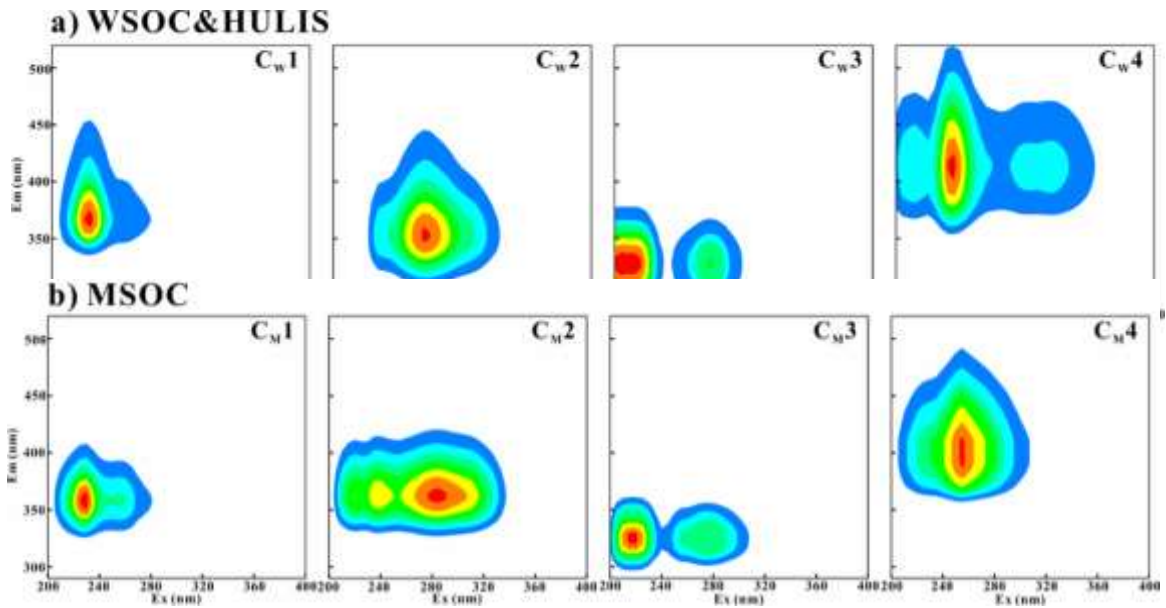


Figure 3. Four fluorescence components identified by PARAFAC analysis of a) WSOC, HULIS ($C_{w1}:C_{w4}$); b) MSOC ($C_{m1}:C_{m4}$) extracted from BB and CC smoke $PM_{2.5}$ (normalized in Raman unit, R.U.)

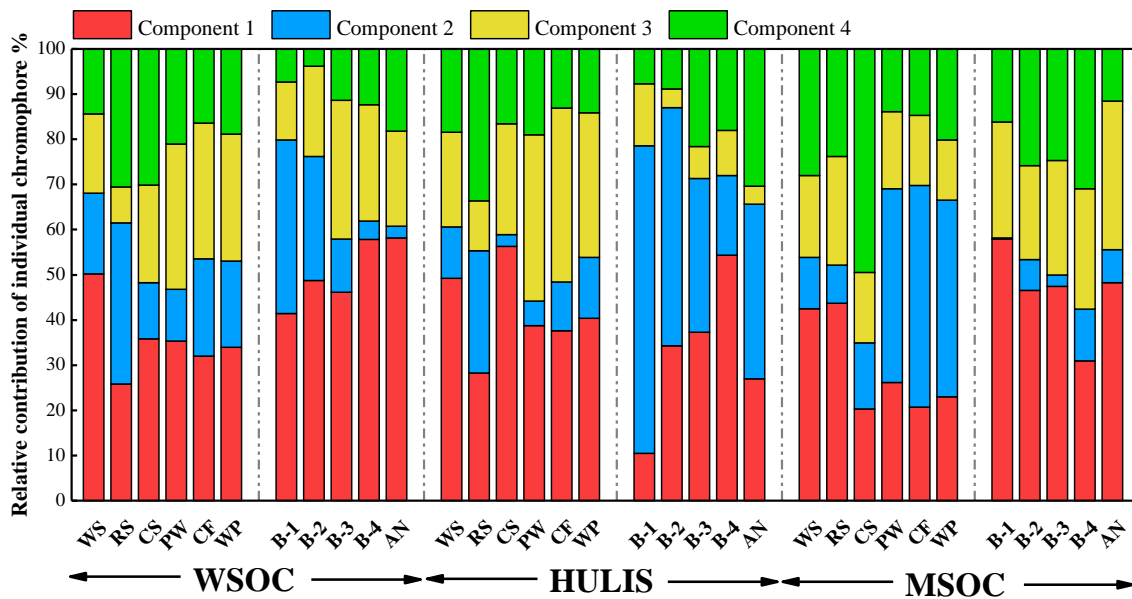


Figure 4. Relative contribution calculated by F_{max} of individual chromophores analyzed by PARAFAC. Component 1-4 represent C_{w1-4} for water-soluble BrC (WSOC and HULIS) and C_{m1-4} for methanol-soluble BrC (MSOC), respectively.

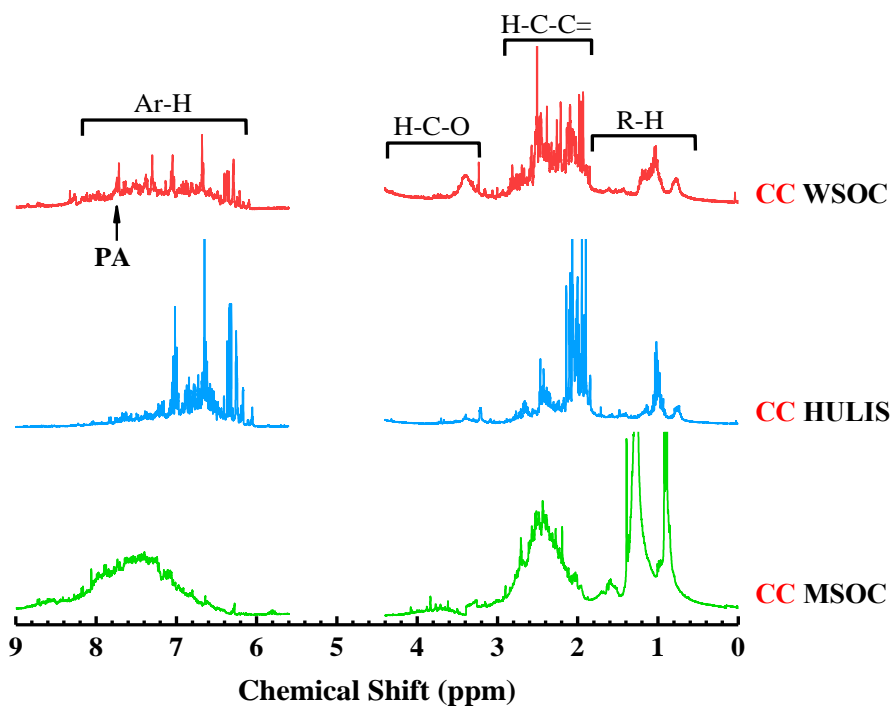
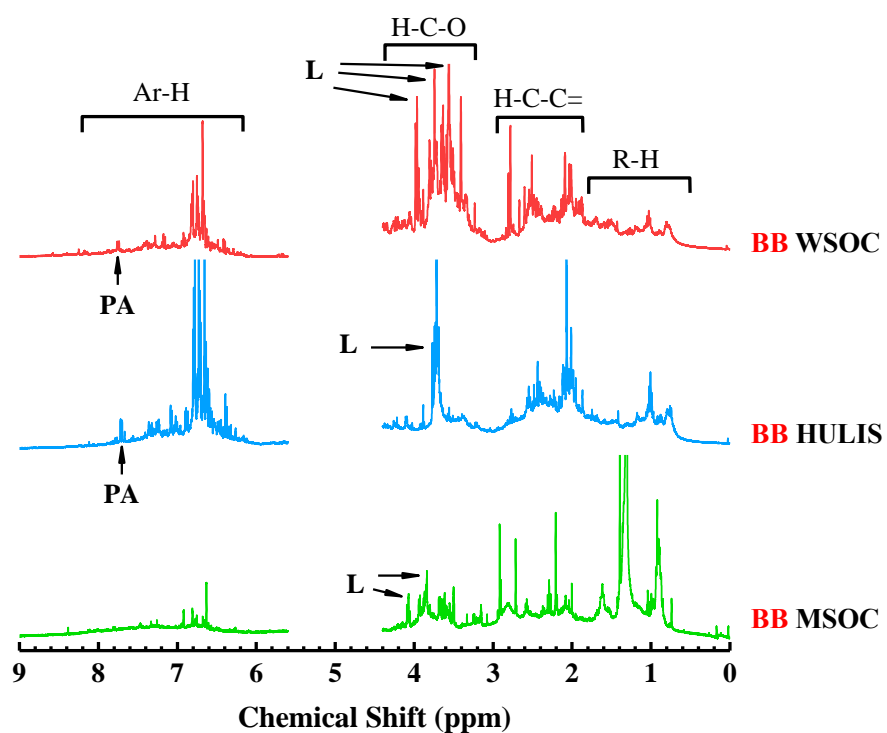


Figure 5. ^1H NMR spectra of WSOC, HULIS, and MSOC in typical biomass burning and coal combustion smoke samples (BB: wheat straw; CC: B-1 coal). The segment from 4.40 to 5.60 ppm was removed for NMR spectra due to MeOH and H_2O residues. The peaks were assigned to specific compounds as follows: Levoglucosan (L), Phthalic acid (PA).

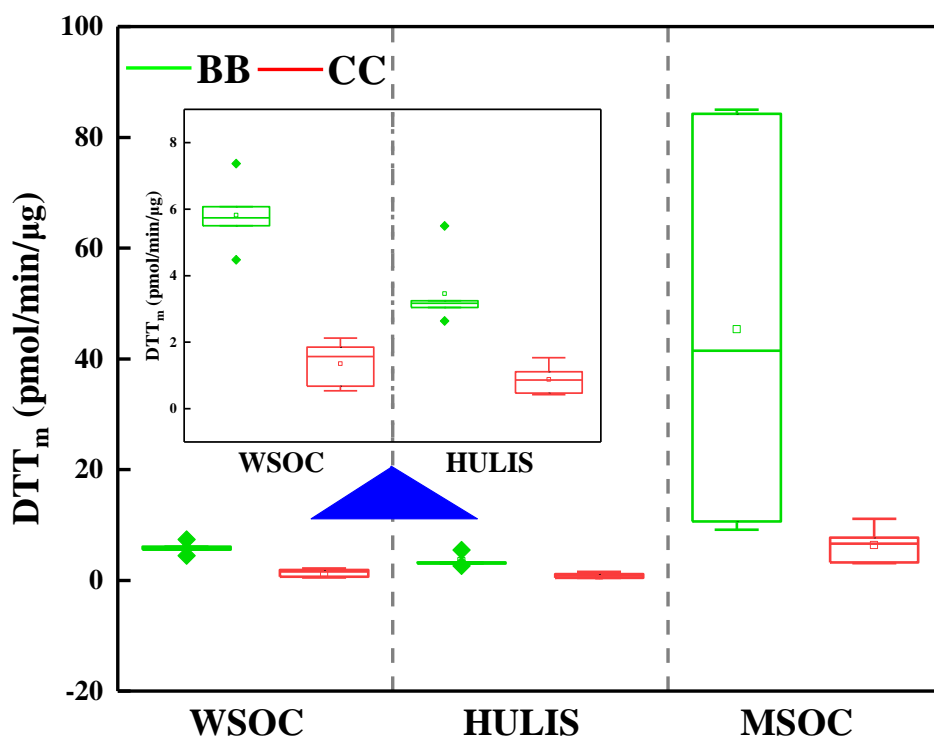


Figure 6. Results of DTT assay conducted on the WSOC, HULIS and MSOC of smoke PM_{2.5}, the values were normalized by the mass of smoke PM_{2.5}. Above the blue triangle symbol is the result coordinates of WSOC and HULIS to be enlarged.

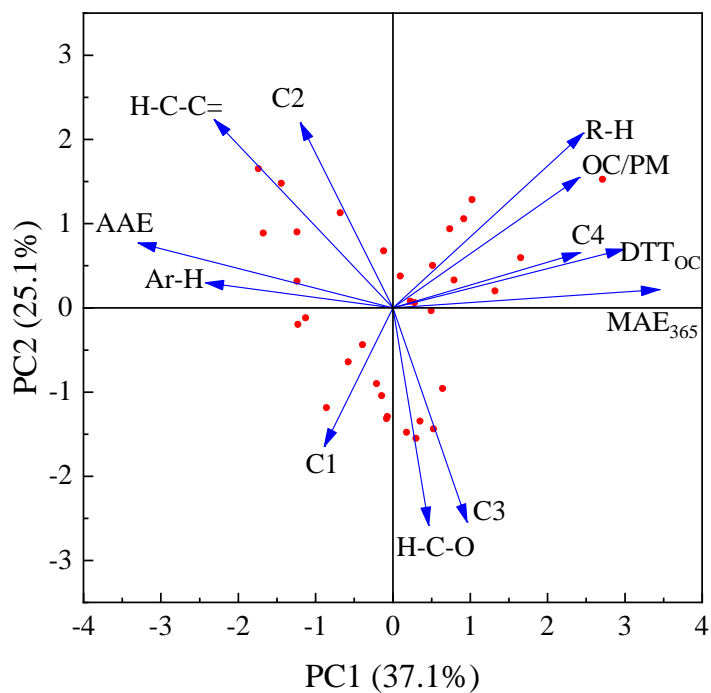


Figure 7. Principal component analysis results for the carbon mass-normalized OP activities and chemical characteristics of BrCs in smoke particles.